LETTER

doi:10.1038/nature16500

Mitofusin 2 maintains haematopoietic stem cells with extensive lymphoid potential

Larry L. Luchsinger[1,2], Mariana Justino de Almeida[1,3], David J. Corrigan[1,3], Melanie Mumau[1,3] & Hans-Willem Snoeck[1,2,3]

Haematopoietic stem cells (HSCs), which sustain production of all blood cell lineages[1], rely on glycolysis for ATP production[2,3], yet little attention has been paid to the role of mitochondria. Here we show in mice that the short isoform of a critical regulator of HSCs, *Prdm16* (refs 4, 5), induces mitofusin 2 (Mfn2), a protein involved in mitochondrial fusion and in tethering of mitochondria to the endoplasmic reticulum. Overexpression and deletion studies, including single-cell transplantation assays, revealed that Mfn2 is specifically required for the maintenance of HSCs with extensive lymphoid potential, but not, or less so, for the maintenance of myeloid-dominant HSCs. Mfn2 increased buffering of intracellular Ca^{2+}, an effect mediated through its endoplasmic reticulum–mitochondria tethering activity[6,7], thereby negatively regulating nuclear translocation and transcriptional activity of nuclear factor of activated T cells (Nfat). Nfat inhibition rescued the effects of *Mfn2* deletion in HSCs, demonstrating that negative regulation of Nfat is the prime downstream mechanism of Mfn2 in the maintenance of HSCs with extensive lymphoid potential. Mitochondria therefore have an important role in HSCs. These findings provide a mechanism underlying clonal heterogeneity among HSCs[8–11] and may lead to the design of approaches to bias HSC differentiation into desired lineages after transplantation.

Within the haematopoietic system, the transcriptional co-regulator, *Prdm16*, is expressed selectively in HSCs and its deletion severely impairs HSC maintenance[4,5]. However, its molecular targets remain unknown. We observed that in *Prdm16*$^{-/-}$ HSCs ($Lin^-Sca1^+Kit^+CD48^-CD150^+Flt3^-$, Extended Data Fig. 1) and mouse embryonic fibroblasts (MEFs) mitochondria were fragmented (Fig. 1a and Extended Data Fig. 2a). Mitochondria undergo dynamic fusion and fission[12,13]. Fusion is driven by the outer membrane GTPases, mitofusin (Mfn) 1 and 2, and by the inner membrane protein optic atrophy 1 (Opa1), while fission requires dynamin-related protein (Drp1)[12,13]. Culture of *Prdm16*$^{-/-}$ MEFs in the presence of the Drp1 inhibitor, mDivi1 (ref. 14), restored mitochondrial length (Extended Data Fig. 2b, c), suggesting a fusion defect, which was further documented in a mitochondrial fusion assay (Extended Data Fig. 2d). Expression of Mfn2 protein and of *Mfn2*, but not *Mfn1*, messenger RNA was lower in *Prdm16*-deficient MEFs and HSCs compared to wild type (Fig. 1b–d and Extended Data Fig. 2e). Furthermore, mitochondria were similarly fragmented in *Prdm16*$^{-/-}$ and in *Mfn2*$^{-/-}$ MEFs (Extended Data Fig. 2f) and mitochondrial length was restored after lentiviral expression of *Mfn2* in *Prdm16*$^{-/-}$ MEFs (Fig. 1e, f and Extended Data Fig. 2g), suggesting that Mfn2 is a target of *Prdm16*.

Prdm16 exists in two isoforms arising from distinct transcription start sites, full-length (fl) and short (s) Prdm16, which lacks the amino-terminal PR-domain (Extended Data Fig. 3a)[15,16]. Only sPrdm16, but not flPrdm16, activated a *Mfn2* promoter luciferase reporter (Extended Data Fig. 3b, c), and induced *Mfn2* mRNA in *Prdm16*$^{-/-}$ MEFs (Fig. 1g). Consistent with these findings, chromatin immunoprecipitation in MEFs using Flag-tagged isoforms of *Prdm16* showed binding of sPrdm16, but not of flPrdm16, to the *Mfn2* promoter (Extended Data Fig. 3d)[17]. *Mfn2* is therefore a direct target of sPrdm16. Although deletion of *Prdm16* did not affect *Mfn1* (Fig. 1b, c), transduction of *sPrdm16* did increase *Mfn1* mRNA expression (Fig. 1g). *Mfn1* is therefore susceptible to regulation by *sPrdm16*, but with a higher and probably unphysiological threshold. Lentiviral transduction of *Mfn2* did not rescue the competitive repopulation defect of *Prdm16*$^{+/-}$ HSCs, however (Extended Data Fig. 3e), indicating that multiple components of the *sPrdm16* and *flPrdm16* transcriptional program are required for HSC maintenance.

Induction of *Mfn2* by *Prdm16*, a critical regulator of HSCs, suggests a role for *Mfn2* in HSC function. We therefore assessed mitochondrial length and Mfn2 expression in haematopoietic cells. HSCs display clonal heterogeneity in their differentiation potential ranging from rare lymphoid-biased HSCs, to balanced myeloid/lymphoid and myeloid-dominant HSCs with low lymphoid potential[8–11]. Although the underlying mechanism is unknown and neither functional nor phenotypic classifications are absolute, myeloid-dominant HSCs are enriched in the $CD150^{hi}$, while HSCs with extensive lymphoid potential are enriched in the $CD150^{lo}$ fraction[18,19]. HSCs expressed more *Mfn2* mRNA (Fig. 2a) and protein (Fig. 2b) than more mature populations. Within the HSC compartment, $CD150^{lo}$ HSCs expressed more Mfn2 mRNA (Fig. 2a) and protein (Fig. 2c) than did $CD150^{hi}$ HSCs. In contrast, *Mfn1* did not show HSC-selective expression, and its expression in $CD150^{lo}$ HSCs was tenfold lower than that of *Mfn2* (Fig. 2a). In accordance with *Mfn2* induction by *sPrdm16*, *sPrdm16* was the predominant *Prdm16* isoform in $CD150^{lo}$ but not in $CD150^{hi}$ HSCs (Fig. 2d). Using mice expressing a mitochondrially targeted Dendra2 fluorescent protein (Pham mice)[20], we observed longer mitochondria in HSCs compared to other haematopoietic populations, and within the HSC compartment, in $CD150^{lo}$ than in $CD150^{hi}$ cells (Fig. 2e and Extended Data Fig. 4a, b). Mitochondrial length therefore paralleled Mfn2 expression.

As these findings suggested a subpopulation-specific role for *Mfn2* in HSCs, we examined mice with conditional deletion of *Mfn2* (ref. 21) in the haematopoietic system (*Mfn2*$^{fl/fl}$-*Vav-Cre*). The frequency of progenitors in the bone marrow and thymus and of mature populations in blood and spleen were similar in *Mfn2*$^{fl/fl}$-*Vav-Cre* mice and *Mfn2*$^{fl/fl}$ littermates (Extended Data Table 1). The $Lin^-Sca1^+Kit^+CD48^-CD150^+$ HSC compartment in *Mfn2*$^{fl/fl}$-*Vav-Cre* mice showed mitochondrial fragmentation (Extended Data Fig. 5a, b), was smaller (Extended Data Table 1) and expressed more CD150 (Extended Data Fig. 5c) compared to that of *Mfn2*$^{fl/fl}$ mice, indicating a loss primarily of $CD150^{lo}$ HSCs. Competitive repopulation studies[22] showed a further increase in CD150 expression within the donor HSC compartment (Extended Data Fig. 5d, e) and a defect in long-term lymphoid repopulation in recipients of *Mfn2*$^{fl/fl}$-*Vav-Cre* adult bone marrow (Fig. 3a) and fetal liver cells (Extended Data Fig. 5f). A decrease in myeloid repopulation was noted, but did not

[1]Columbia Center for Translational Immunology, Columbia University Medical Center, New York, New York 10032, USA. [2]Department of Medicine, Columbia University Medical Center, New York, New York 10032, USA. [3]Department of Microbiology and Immunology, Columbia University Medical Center, New York, New York 10032, USA.

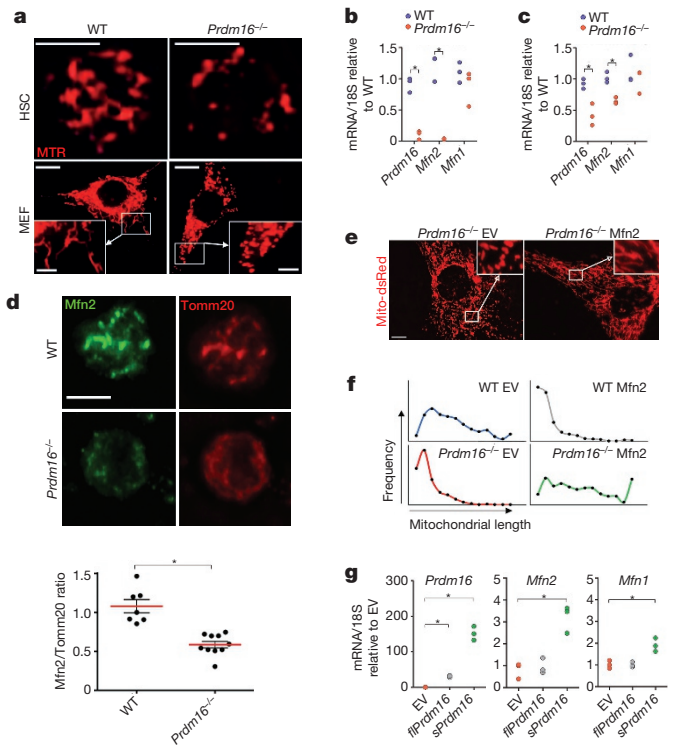

Figure 1 | Prdm16 induces Mfn2. a, Mitochondrial morphology of MTR-stained wild-type (WT) and *Prdm16*$^{-/-}$ fetal liver HSCs ($Lin^-Sca1^+kit^+CD48^-CD150^+Flt3^-$) (scale bars, 5 μm) and MEFs (scale bars, 20 μm; inset, 5 μm). **b**, Relative mRNA expression of *Prdm16*, *Mfn1* and *Mfn2* in WT and *Prdm16*$^{-/-}$ MEFs. $n = 3$ independent experiments; $^*P < 0.05$; two-tailed Student's *t*-test. **c**, Relative mRNA expression of *Prdm16*, *Mfn1* and *Mfn2* in WT and *Prdm16*$^{+/-}$ adult HSCs. $n = 3$ biological replicates; $^*P < 0.05$; two-tailed Student's *t*-test. **d**, Representative immunofluorescence for Mfn2 and Tomm20 in WT and *Prdm16*$^{-/-}$ HSCs (scale bar, 5 μm) and Mfn2 quantification normalized to Tomm20. Bars, mean ± s.e.m.; $n \geq 10$ fields of cells from two biological replicates; $^*P < 0.05$; two-tailed Student's *t*-test. **e**, Mitochondrial morphology in *Prdm16*$^{-/-}$ MEFs co-transduced with Mito-dsRed and Mfn2 or control lentivirus (EV, empty vector) (scale bar, 20 μm). **f**, Mitochondrial length profiles in WT and *Prdm16*$^{-/-}$ MEFs transduced with EV or Mfn2 (≥12 cells and ≥80 mitochondria from 2 biological replicates). Note that Mfn2 overexpression in WT MEFs causes aggregation of mitochondria and apparent shortening, as reported previously[30]. **g**, Relative mRNA expression in *Prdm16*$^{-/-}$ MEFs of *Prdm16*, *Mfn1* and *Mfn2* 72 h after retroviral expression of *sPrdm16* and *flPrdm16*. $n = 3$ biological replicates; $^*P < 0.05$; one-way analysis of variance (ANOVA) with Dunnett's post-hoc test.

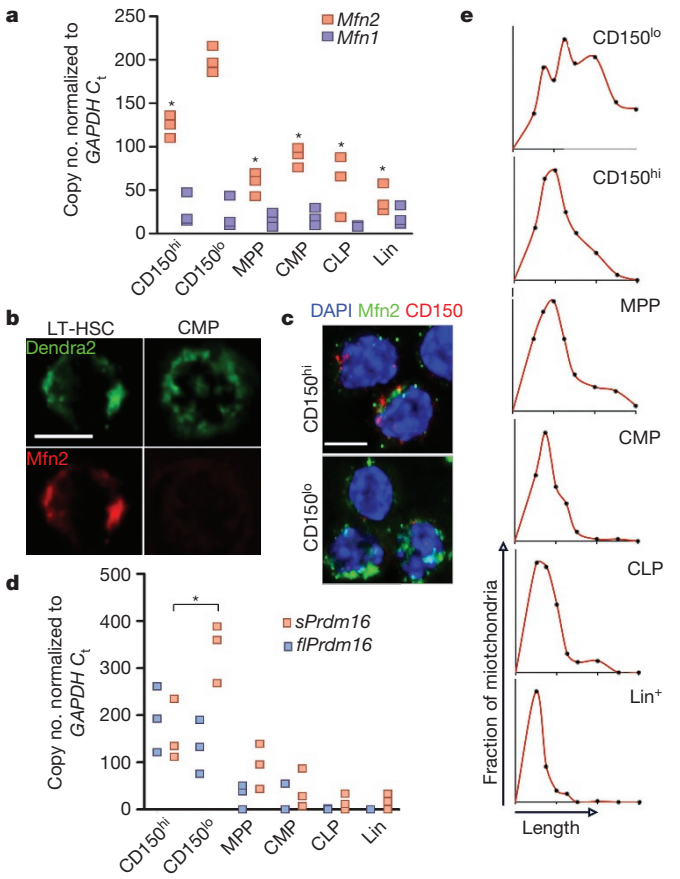

Figure 2 | Mitochondrial morphology and Mfn2 in HSCs. a, Expression of *Mfn2* and *Mfn1* mRNA in HSCs, progenitors (MPP, multipotential progenitors, $Lin^-Sca1^+kit^+CD150^-Flt3^+$; CMP, common myeloid progenitors, $Lin^-Sca1^-Kit^+$; CLP, common lymphoid progenitor, $Lin^-Sca1^{lo}kit^{lo}Flt3^+IL7R\alpha^+$ and Lin, lineage$^+$ cells). $n = 3$ biological replicates; $^*P < 0.05$; one-way ANOVA with Dunnett's post-hoc test. **b**, Mfn2 immunofluorescence in Pham-reporter$^+$ HSCs and CMPs (Pham mice express a mitochondrially targeted Dendra2 fluorescent protein[20]) (scale bar, 5 μm). **c**, Immunofluorescence staining for Mfn2 and CD150 in $CD150^{hi}$ and $CD150^{lo}$ $LSKCD48^-$ HSCs (scale bar, 5 μm). Cell nuclei counterstained with DAPI. **d**, Quantification of *flPrdm16* and *sPrdm16* mRNA in HSCs, progenitors and Lin$^+$ cells. $n = 3$ biological replicates; $^*P < 0.05$; one-way ANOVA with Dunnett's post-hoc test. **e**, Mitochondrial length frequency profile in Pham-reporter$^+$ HSCs, progenitors and Lin$^+$ cells ($n \geq 15$ fields from three biological replicates).

reach statistical significance (Fig. 3a and Extended Data Fig. 5f). Lentiviral overexpression of *Mfn2* in wild-type HSCs yielded reciprocal results (Extended Data Fig. 6a–i). As these phenotypic analyses and transplantation experiments suggested selective requirement for *Mfn2* in the maintenance of HSCs with extensive lymphoid potential, we performed competitive single HSC transplantation studies to rigorously determine clonal variation in differentiation potential. Although out of >100 recipients too few mice were reconstituted to statistically assess HSC frequency, among recipients with >0.1% donor contribution most *Mfn2*$^{fl/fl}$*-Vav-Cre* HSCs were myeloid-dominant, whereas most *Mfn2*$^{fl/fl}$ HSCs were balanced or lymphoid 8 weeks after transplantation. In mice that still showed repopulation after 13 weeks, only myeloid-dominant HSCs were detected recipients of *Mfn2*$^{fl/fl}$*-Vav-Cre*, while most donor HSCs had extensive lymphoid potential in recipients of *Mfn2*$^{fl/fl}$ cells (Fig. 3b). To more accurately determine HSC frequencies we performed limiting dilution experiments[22]. Among *Mfn2*$^{fl/fl}$*-Vav-Cre* HSCs overall repopulating HSC frequency was decreased fourfold compared to *Mfn2*$^{fl/fl}$ HSC (Fig. 3c and Extended Data Table 2). The frequency of HSCs capable of >1% long-term lymphoid reconstitution was also approximately fourfold lower. However, the decrease in the frequency of HSCs capable of >1% myeloid reconstitution did not reach statistical significance (Fig. 3c and Extended Data Table 2). Taken together, these results indicate that *Mfn2* is required for the maintenance of HSCs with extensive lymphoid potential.

Next, we identified the mechanism of action of Mfn2. Apoptosis and reactive oxygen species production were similar in *Mfn2*$^{fl/fl}$*-Vav-Cre* and *Mfn2*$^{fl/fl}$ HSCs, but *Mfn2*$^{fl/fl}$*-Vav-Cre* HSCs and progenitors displayed increased expression of Grp78, a marker of endoplasmic reticulum stress, which has been shown to be associated with *Mfn2* deletion[23] (Extended Data Fig. 7a–c). *Mfn2*, but not *Mfn1*, also tethers mitochondria to the endoplasmic reticulum, thereby enhancing intracellular calcium buffering[6]. Indeed, intracellular Ca^{2+} was increased in *Mfn2*$^{fl/fl}$*-Vav-Cre* compared to *Mfn2*$^{fl/fl}$ HSCs (Fig. 4a), in $CD150^{hi}$ compared to $CD150^{lo}$ HSCs (Fig. 4b) and in *Prdm16*$^{-/-}$ compared to wild-type LSK cells (Fig. 4c), but was decreased after lentiviral transduction of wild-type HSCs (Extended Data Fig. 7d). However, Mfn2 did not affect ATP- or SDF1-induced intracellular Ca^{2+} transients (Fig. 4a–c and Extended Data Fig. 7d). At variance with these data

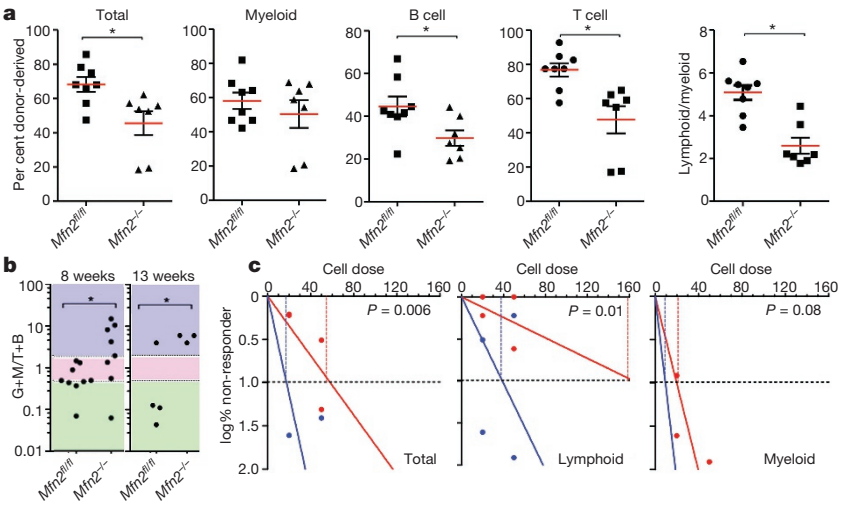

Figure 3 | Role of Mfn2 in HSC function. a, Donor (CD45.2) chimaerism 15 weeks after competitive transplantation of 2×10^5 *Mfn2*$^{fl/fl}$ or *Mfn2*$^{fl/fl}$.*Vav-Cre* (*Mfn2*$^{-/-}$) adult bone marrow cells together with 2×10^5 CD45.1$^+$ competitor bone marrow cells into CD45.1$^+$CD45.2$^+$ recipients. Plots, mean ± s.e.m.; $n = 7$–8 recipients from two independent transplants; $^*P < 0.05$; two-tailed Student's *t*-test. **b**, Donor GM/B+T reconstitution ratios 8 (left) and 13 (right) weeks after transplantation of single HSCs from *Mfn2*$^{fl/fl}$ or *Mfn2*$^{fl/fl}$.*Vav-Cre* (*Mfn2*$^{-/-}$) mice. Plots, mean ± s.e.m.; $n \geq 8$ recipients; $^*P < 0.05$; Student's *t*-test. Colours represent myeloid-biased (blue), balanced (pink) and lymphoid dominant (green) as defined in ref. 11. **c**, Limiting dilution assay (see Methods) with *Mfn2*$^{fl/fl}$ or *Mfn2*$^{fl/fl}$.*Vav-Cre* (*Mfn2*$^{-/-}$) adult bone marrow HSCs co-transplanted with CD45.1$^+$ competitor bone marrow cells analysed for total, myeloid or lymphoid potential 15 weeks after transplantation. Plots, log% negative responders; $n = 2$ independent experiments with 4–5 recipients each per cell dose; frequencies calculated using limiting dilution analysis Poisson distribution; $P < 0.05$; Pearson's chi-squared test.

and with a previous report showing only delayed removal of intracellular Ca^{2+} (ref. 6), we found both lower baseline intracellular Ca^{2+} and lower amplitude of ATP-induced calcium flux in *Mfn2*$^{-/-}$ MEFs (Extended Data Fig. 7e). Thus, despite cell type-specific differences in calcium homeostasis, *Mfn2* negatively regulates intracellular Ca^{2+}.

Sustained increase in intracellular Ca^{2+} activates calcineurin, which dephosphorylates four isoforms of Nfat and promotes their translocation to the nucleus[24], where they orchestrate multiple processes[25,26]. We therefore examined whether Mfn2 inhibits Nfat. As measured by immunofluorescence, Nfat1 nuclear localization was decreased after lentiviral transduction of wild-type HSCs (Extended Data Fig. 7f), and increased in *Mfn2*$^{fl/fl}$-*Vav-Cre* compared to *Mfn2*$^{fl/fl}$ HSCs (Fig. 4d) and in *Mfn2*$^{-/-}$ compared to wild-type MEFs (Extended Data Fig. 7g), which was confirmed by cellular fractionation followed by western blot (Fig. 4e). Consistent with inhibition of Nfat nuclear localization by Mfn2, the fraction of nuclear Nfat was also higher in CD150^{hi} compared to CD150^{lo} HSCs (Fig. 4f) and in *Prdm16*$^{-/-}$ compared to wild-type HSCs (Fig. 4g). We next assessed the effect of

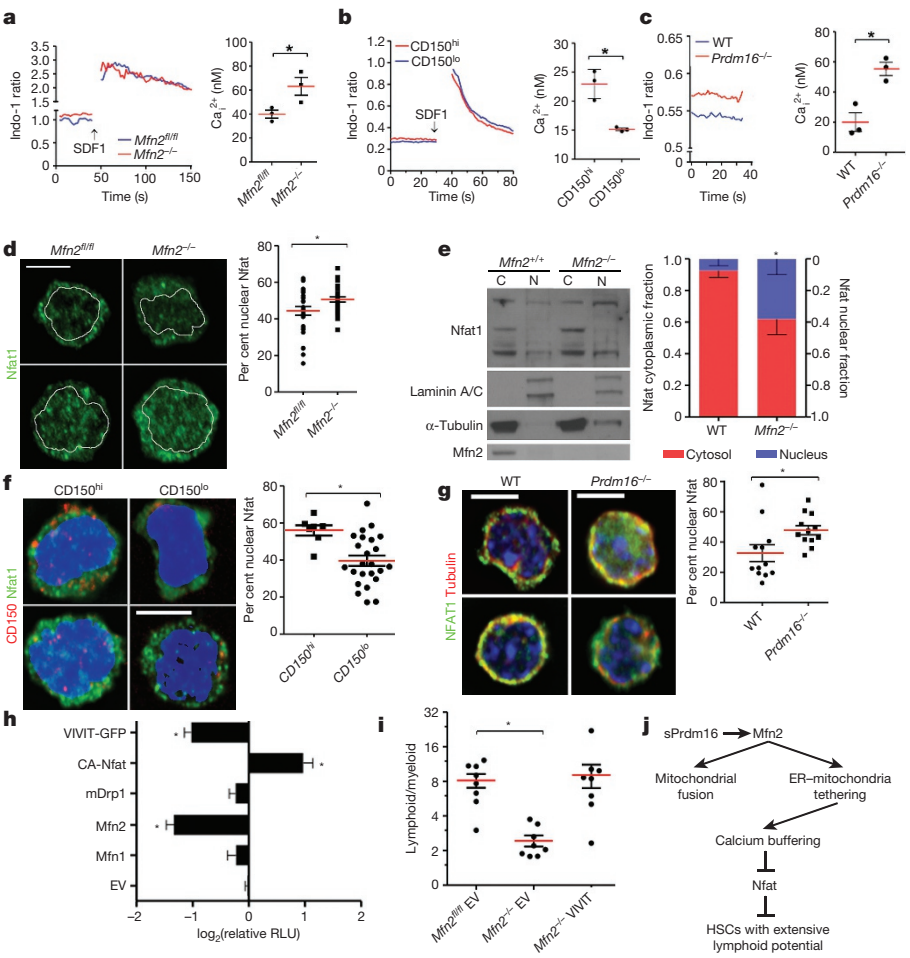

Figure 4 | Mechanism of action of Mfn2. **a**–**c**, Calcium flux trace (left) and baseline intracellular Ca^{2+} (right) in *Mfn2*$^{fl/fl}$ or *Mfn2*$^{fl/fl}$.*Vav-Cre* (*Mfn2*$^{-/-}$) HSCs (**a**), CD150^{hi} and CD150^{lo} HSCs (**b**), and WT and *Prdm16*$^{-/-}$ HSCs (**c**). Plots, mean ± s.e.m.; $n = 3$ biological replicates; $^*P < 0.05$; two-tailed Student's *t*-test. **d**, Nfat1 staining (left; scale bar, 5 μm) and percentage of nuclear Nfat1 (right, $^*P < 0.05$) in *Mfn2*$^{fl/fl}$ or *Mfn2*$^{fl/fl}$.*Vav-Cre* (*Mfn2*$^{-/-}$) HSCs. Plot, mean ± s.e.m.; $n \geq 7$ fields of cells from two biological replicates; $^*P < 0.05$; two-tailed Student's *t*-test. **e**, Subcellular fractionation followed by western blot for Nfat1 in WT and *Mfn2*$^{-/-}$ MEFs (left, see Supplementary Fig. 1 for full scan) and relative quantification of nuclear and cytoplasmic fraction (right). Bars, mean ± s.d.; $n = 3$ biological replicates; $^*P < 0.05$; two-tailed Student's *t*-test. **f**, **g**, Nfat1 staining (left, scale bars = 5 μm) and percentage of nuclear Nfat1 (right, $^*P < 0.05$) in CD150^{hi} and CD150^{lo} HSCs (**f**), and WT and *Prdm16*$^{-/-}$ fetal liver HSCs (**g**). Plots, mean ± s.e.m.; $n \geq 7$ fields of cells pooled from three biological replicates; $^*P < 0.05$; two-tailed Student's *t*-test. **h**, Luciferase activity of 3×Nfat gene reporter in 3T3 cells transfected with constructs on *y* axis (EV, empty vector). Data normalized to β-Gal activity and relative to EV. CA-Nfat, constitutively active Nfat; RLU, relative light units. Bars, mean ± s.d.; $n = 7$ biological replicates; $^*P < 0.05$; one-way ANOVA with Dunnett's post-hoc test. **i**, Lymphoid/myeloid ratio 15 weeks after competitive transplantation of *Mfn2*$^{fl/fl}$ or *Mfn2*$^{fl/fl}$.*Vav-Cre* (*Mfn2*$^{-/-}$) HSCs transduced with IRES–GFP (EV) or VIVIT–GFP. Plots, mean ± s.e.m.; $n > 8$ recipients pooled from three independent transplants; $^*P < 0.05$; one-way ANOVA with Dunnett's post-hoc test. **j**, Schematic representation of the mechanism of action of Mfn2.

Mfn2 on Nfat transcriptional activity. Transfection of *Mfn2*$^{-/-}$ MEFs with a Nfat-responsive luciferase reporter revealed increased Nfat transcriptional activity compared to wild-type MEFs (Extended Data Fig. 7h). Conversely, overexpression of *Mfn2* in NIH-3T3 fibroblasts reduced Nfat-responsive luciferase reporter activity to the same extent as VIVIT, a membrane-permeable peptide that specifically inhibits the interaction between calcineurin and Nfat (Fig. 4h)[27]. However, *Mfn1* and a dominant negative DRP1 mutant (Extended Data Fig. 7i) had no effect (Fig. 4h). Unlike *Mfn2*, *Mfn1* and *Drp1* only regulate mitochondrial fusion and fission. These findings therefore suggest that Mfn2 inhibits Nfat through its endoplasmic reticulum–mitochondria tethering activity rather than through mitochondrial fusion. Finally, and consistent with *Mfn2* induction by *sPrdm16*, lentiviral transduction of *Prdm16*$^{-/-}$ HSCs with *sPrdm16*, but not with *flPrdm16*, reduced Nfat nuclear localization (Extended Data Fig. 7j), while Nfat transcriptional activation was increased in *Prdm16*$^{-/-}$ MEFs and normalized by transfection of either *sPrdm16* or *Mfn2*, but not *flPrdm16* (Extended Data Fig. 7k). We conclude that *sPrdm16*-mediated induction of *Mfn2* inhibits Nfat activity.

To directly examine the role of Nfat downstream of *Mfn2*, we inhibited its function in HSCs. Culture of wild-type HSCs in the presence of VIVIT peptide increased expression of CD150^{lo} HSC-associated lymphoid commitment markers, *Il7r* and *Sox4* (ref. 18; Extended Data Fig. 8a), and increased lymphoid/myeloid repopulation ratio after subsequent competitive transplantation (Extended Data Fig. 8b). Most importantly, lentiviral VIVIT–GFP[27] transduction fully rescued the long-term lymphoid reconstitution defect of *Mfn2*$^{fl/fl}$*-Vav-Cre* HSCs (Fig. 4i) and, similar to Mfn2 transduction, increased lymphoid repopulation of wild-type HSCs (Extended Data Fig. 8c). Nfat inhibition is therefore the prime mechanism downstream of *Mfn2*.

The observation that *Mfn2*, induced by s*Prdm16*, maintains HSCs with extensive lymphoid potential by negatively regulating calcineurin/Nfat activity through enhanced intracellular Ca^{2+} buffering (Fig. 4l) identifies such HSCs, which decline with age[28,29], as a mechanistically defined subset and provides a mechanism underpinning clonal heterogeneity in HSCs. These findings may lead to the design of approaches to bias HSC differentiation into desired lineages after transplantation.

Online Content Methods, along with any additional Extended Data display items and Source Data, are available in the online version of the paper; references unique to these sections appear only in the online paper.

Received 15 January; accepted 30 November 2015.
Published online 20 January 2016.

1. Orkin, S. H. & Zon, L. I. Hematopoiesis: an evolving paradigm for stem cell biology. *Cell* **132,** 631–644 (2008).
2. Simsek, T. *et al.* The distinct metabolic profile of hematopoietic stem cells reflects their location in a hypoxic niche. *Cell Stem Cell* **7,** 380–390 (2010).
3. Takubo, K. *et al.* Regulation of glycolysis by Pdk functions as a metabolic checkpoint for cell cycle quiescence in hematopoietic stem cells. *Cell Stem Cell* **12,** 49–61 (2013).
4. Aguilo, F. *et al.* Prdm16 is a physiologic regulator of hematopoietic stem cells. *Blood* **117,** 5057–5066 (2011).
5. Chuikov, S., Levi, B. P., Smith, M. L. & Morrison, S. J. Prdm16 promotes stem cell maintenance in multiple tissues, partly by regulating oxidative stress. *Nature Cell Biol.* **12,** 999–1006 (2010).
6. de Brito, O. M. & Scorrano, L. Mitofusin 2 tethers endoplasmic reticulum to mitochondria. *Nature* **456,** 605–610 (2008).
7. Rizzuto, R., De Stefani, D., Raffaello, A. & Mammucari, C. Mitochondria as sensors and regulators of calcium signalling. *Nature Rev. Mol. Cell Biol.* **13,** 566–578 (2012).
8. Müller-Sieburg, C. E., Cho, R. H., Thoman, M., Adkins, B. & Sieburg, H. B. Deterministic regulation of hematopoietic stem cell self-renewal and differentiation. *Blood* **100,** 1302–1309 (2002).
9. Sanjuan-Pla, A. *et al.* Platelet-biased stem cells reside at the apex of the haematopoietic stem-cell hierarchy. *Nature* **502,** 232–236 (2013).
10. Muller-Sieburg, C. E. & Sieburg, H. B. Clonal diversity of the stem cell compartment. *Curr. Opin. Hematol.* **13,** 243–248 (2006).
11. Dykstra, B. *et al.* Long-term propagation of distinct hematopoietic differentiation programs *in vivo*. *Cell Stem Cell* **1,** 218–229 (2007).
12. Chan, D. C. Fusion and fission: interlinked processes critical for mitochondrial health. *Annu. Rev. Genet.* **46,** 265–287 (2012).
13. Youle, R. J. & van der Bliek, A. M. Mitochondrial fission, fusion, and stress. *Science* **337,** 1062–1065 (2012).
14. Tanaka, A. & Youle, R. J. A chemical inhibitor of DRP1 uncouples mitochondrial fission and apoptosis. *Mol. Cell* **29,** 409–410 (2008).
15. Shing, D. C. *et al.* Overexpression of sPRDM16 coupled with loss of p53 induces myeloid leukemias in mice. *J. Clin. Invest.* **117,** 3696–3707 (2007).
16. Yoshida, M. *et al.* Aberrant expression of the *MEL1S* gene identified in association with hypomethylation in adult T-cell leukemia cells. *Blood* **103,** 2753–2760 (2004).
17. Sorianello, E. *et al.* The promoter activity of human *Mfn2* depends on Sp1 in vascular smooth muscle cells. *Cardiovasc. Res.* **94,** 38–47 (2012).
18. Beerman, I. *et al.* Functionally distinct hematopoietic stem cells modulate hematopoietic lineage potential during aging by a mechanism of clonal expansion. *Proc. Natl Acad. Sci. USA* **107,** 5465–5470 (2010).
19. Weksberg, D. C., Chambers, S. M., Boles, N. C. & Goodell, M. A. CD150- side population cells represent a functionally distinct population of long-term hematopoietic stem cells. *Blood* **111,** 2444–2451 (2008).
20. Pham, A. H., McCaffery, J. M. & Chan, D. C. Mouse lines with photo-activatable mitochondria to study mitochondrial dynamics. *Genesis* **50,** 833–843 (2012).
21. Chen, H., McCaffery, J. M. & Chan, D. C. Mitochondrial fusion protects against neurodegeneration in the cerebellum. *Cell* **130,** 548–562 (2007).
22. Szilvassy, S. J., Humphries, R. K., Lansdorp, P. M., Eaves, A. C. & Eaves, C. J. Quantitative assay for totipotent reconstituting hematopoietic stem cells by a competitive repopulation strategy. *Proc. Natl Acad. Sci. USA* **87,** 8736–8740 (1990).
23. Ngoh, G. A., Papanicolaou, K. N. & Walsh, K. Loss of mitofusin 2 promotes endoplasmic reticulum stress. *J. Biol. Chem.* **287,** 20321–20332 (2012).
24. Li, H., Rao, A. & Hogan, P. G. Interaction of calcineurin with substrates and targeting proteins. *Trends Cell Biol.* **21,** 91–103 (2011).
25. Müller, M. R. *et al.* Requirement for balanced Ca/NFAT signaling in hematopoietic and embryonic development. *Proc. Natl Acad. Sci. USA* **106,** 7034–7039 (2009).
26. Wu, H., Peisley, A., Graef, I. A. & Crabtree, G. R. NFAT signaling and the invention of vertebrates. *Trends Cell Biol.* **17,** 251–260 (2007).
27. Aramburu, J. *et al.* Affinity-driven peptide selection of an NFAT inhibitor more selective than cyclosporin A. *Science* **285,** 2129–2133 (1999).
28. Benz, C. *et al.* Hematopoietic stem cell subtypes expand differentially during development and display distinct lymphopoietic programs. *Cell Stem Cell* **10,** 273–283 (2012).
29. Dykstra, B., Olthof, S., Schreuder, J., Ritsema, M. & de Haan, G. Clonal analysis reveals multiple functional defects of aged murine hematopoietic stem cells. *J. Exp. Med.* **208,** 2691–2703 (2011).
30. Chen, H. *et al.* Mitofusins Mfn1 and Mfn2 coordinately regulate mitochondrial fusion and are essential for embryonic development. *J. Cell Biol.* **160,** 189–200 (2003).

Supplementary Information is available in the online version of the paper.

Acknowledgements The pHR-IRES-GFP SIN vector was a gift from R. Creusot. *Mfn2*$^{-/-}$ MEFs were a gift from D. Chan. We thank S.-H. Ho and E. A. Schon for assistance and discussion. This work was supported by grant NIH RO1 CA167286 and RO1 AG029262 (H.-W.S.), the Druckenmiller Fellowship from the New York Stem Cell Foundation (L.L.L.), the Ruth L. Kirschstein F31 CA196045 fellowship (D.J.C.), the NIH National Center for Research Resources award 1S10RR027050-01 and the NIH Office of the Director award 1S10OD020056-01.

Author Contributions L.L.L. designed and performed most experiments, contributed to the concept, and co-wrote the manuscript with H.-W.S.; M.J.A. generated the data in Fig. 4e and Extended Data Fig. 8a, and assisted in Figs 2, 4i and Extended Data Figs 6–8. M.M. cloned the DNDrp1 construct and verified its function (Extended Data Fig. 7d). D.J.C. generated the Mfn2 promoter construct (Extended Data Fig. 3c). H.-W.S. provided concept and guidance, and co-wrote the paper with L.L.L.

Author Information Reprints and permissions information is available at www.nature.com/reprints. The authors declare no competing financial interests. Readers are welcome to comment on the online version of the paper. Correspondence and requests for materials should be addressed to H.-W.S. (hs2680@columbia.edu).

METHODS

Animals. C57BL/6J mice (CD45.2) and B6.SJL-Ptprca$^{Pep3b/BoyJ}$ (CD45.1) were purchased from The Jackson Laboratory (Bar Harbour, ME). Prdm16$^{Gt(OST67423)Lex}$ knockout mice[31] were obtained from Lexicon Genetics. Conditional Mito-Dendra2 transgenic (Pham) mice[32] (B6;129S-Gt(ROSA)26Sor$^{tm1(CAG-COX8A/Dendra2)Dcc/J}$) and E2A-Cre mice[33] (B6.FVB-Tg(EIIa-cre)C5379Lmgd/J) were purchased from Jackson Laboratory. Pham mice contain a mitochondrially targeted Dendra preceded by a stoplox sequence in the Rosa locus. These mice were crossed with E2A-Cre mice to effect ubiquitous induction of the MitoDendra2 reporter. Conditional Mfn2 knockout mice[34] (B6/129SF1$^{Mfn2tm3Dcc/Mmucd}$) were obtained from MMRRC and crossed to Vav-Cre transgenic mice[35] (B6.Cg-Tg(Vav1-Cre)A2Kio/J) to obtain a homozygous floxed allele *Mfn2* allele which generated a B6.Cg-Tg(Vav1-Cre)A2Kio/J;B6/126SF1 $^{Mfn2tm3Dcc/Mmucd}$ mixed mouse strain. All mouse strains were rederived by *in vitro* fertilization at the Jackson Laboratory. Animals were housed in a specific pathogen-free facility. Experiments and animal care were performed in accordance with the Columbia University Institutional Animal Care and Use Committee. All mice were used at age 8–12 weeks, except in experiments that involved fetal liver cells, when E14.4 embryos were used. Both sexes were used for experiments. Results were analysed in non-blinded fashion. In all experiments, randomly chosen wild type and littermates were used.

MEF isolation and cell lines. MEFs were established from approximately 14.5 days post coitum embryos as previously described[36] from *Prdm16*$^{+/-}$ breeder pairs. Briefly, dissected embryo trunks were minced into 1–2 mm fragments, resuspended in 3 ml 0.25% trypsin/EDTA (Gibco, Carlsbad, CA) and passed 20–30 times through a 16 gauge needle. Cell suspensions were incubated at 37 °C for 1 h with frequent agitation. Erythrocytes were lysed with ACK buffer, washed and cells were plated for 3 h in 10% FBS/DMEM. Cells remaining in suspension were aspirated and adherent cells were cultured with fresh media. MEFs were passaged 1:3 every 3 days and cells between passage 2 and 5 were used for all experiments. 293 cells and NIH-3T3 cells were purchased from ATCC (Manassas, VA) and sub-cultured in 10% FBS/DMEM or 10% calf serum/DMEM, respectively. WT and *Mfn2*$^{-/-}$ MEFs were a kind gift from E. Schon (Columbia University). All lines are tested yearly for mycoplasma contamination and found negative.

Plasmids. *Prdm16* constructs were generated by subcloning the murine full length (*flPrdm16*) or truncated (*sPrdm16*) cDNA into the XhoI/EcoRI sites of the pMSCV-IRES-GFP retroviral expression plasmid. The Mito-dsRed construct was purchased from Addgene (Cambridge, MA) (plasmid 11151). *Mfn2* constructs were generated by subcloning the murine *Mfn2* cDNA into the EcoRI/BamHI sites of the pLVX-EF1α-IRES-GFP or pLVX-EF1α-IRES-mCherry lentiviral expression plasmid (Clontech). The pGreenFire-Nfat and pGreenFire-CMV gene reporter constructs were purchased from System Biosciences (San Jose, CA) and contained three canonical Nfat response elements (5′-GGAAAAN-3′) driving the expression of copGFP and luciferase reporters. The DNDrp1-pcDNA3.1 construct was purchased from Addgene (#45161) and subcloned using the BamHI/EcoRI restriction sites into the pLVX-IRES-GFP vector. Lentiviral 2nd generation packaging construct ΔR8.2 (8455) and pDM2.6 (12259) were purchased from Addgene. The −950/+22 murine *MFN2* promoter was constructed by PCR amplification of the RP23-458J18 BAC clone (CHORI, Oakland, CA) and subcloned into the pGL4 luciferase reporter vector (Promega, Madison, WI). All cloning was carried out using KOD hot-start polymerase (Novagen, Billerica, MA) and subcloned for screening and sequencing into the pCR2.1 shuttle vector (Invitrogen, Carlsbad, CA).

FACS sorting and analysis. For peripheral blood analyses, erythrocytes were lysed twice with ACK lysis buffer and nucleated cells were stained with antibody cocktail (Supplementary Table 1) in FACS buffer for 15 min on ice, washed and analysed on a BD FACSCantoII flow cytometer (Becton Dickinson, Mountain View, CA). For bone marrow analyses, cells were isolated using the crushing method and erythrocytes were lysed with ACK lysis buffer followed by 40 μm filtration. bone marrow cells were stained with antibody cocktail in FACS buffer for 30 min on ice, washed and analysed on a BD LSRII flow cytometer (Becton Dickinson, Mountain View, CA). Dead cells were excluded from analyses by gating out 7AAD-positive cells. To isolate purified haematopoietic populations, bone marrow cells were isolated, stained and sorted using a BD Influx cell sorter (Becton Dickinson, Mountain View, CA) into complete media. Data were analysed using FlowJo9.6 (TreeStar Inc., Ashland, OR).

Haematopoietic stem cell transplantation. *Mfn2*$^{fl/fl}$*-Vav-Cre* fetal liver cells, bone marrow cells or purified LT-HSCs (Lin$^-$cKit$^+$Sca1$^+$CD48$^-$Flt3$^-$CD150$^+$) were transplanted into lethally irradiated (two doses of 478 cGy over 3 h using a Rad Source RS-2000 X-ray irradiator (Brentwood, TN)) recipients together with 2×10^5 competitor cells. As *Mfn2*$^{fl/fl}$*-Vav-Cre* mice were not fully backcrossed onto the C57BL/6 background, recipient mice and competitor bone marrow cells were from the B6.Cg-Tg(Vav1-Cre)A2Kio/J;B6/126SF1 $^{Mfn2tm3Dcc/Mmucd}$ mixed background mouse strain crossed to B6.SJL-Ptprca Pep3b/BoyJ (CD45.1) to generate a CD45.1$^+$CD45.2$^+$ mixed background mouse. Competitor cells were T-cell depleted using MACS beads. For all competitive transplantation experiments, at least two independent transplants, each with at least 4 recipients per condition of genotype were performed, and result of all recipients pooled for statistical analysis. Power calculation was based on results of the first experiment. In limiting dilution assays, cohorts of recipients received 20 or 50 HSCs together with 2×10^5 competitor cells, allowing calculation of HSC frequency based on the number of non-repopulated mice (<1% donor contribution) using Poisson statistics 15 weeks after reconstitution. For Mfn2 KO single cell transplantation, LT-HSCs were sorted directly into complete media (StemPro34, 100 ng ml^{-1} SCF, 100 ng ml^{-1} TPO, 50 ng ml^{-1} IL-6) and single cells were visually confirmed. Positive single cell wells were combined with 2×10^5 CD45.1 competitor bone marrow cells and transplanted into lethally irradiated CD45.1 recipient mice. Recipients showing ≥0.1% CD45.2 donor contribution were considered positive and GM/(B+T) ratios were calculated as previously described for characterizing heterogeneous HSC phenotypes[37]. In transplantations using WT or *Prdm16*$^{-/-}$ HSCs (Lin$^-$cKit$^+$Sca1$^+$CD48$^-$Flt3$^-$CD150$^+$) B6.CD45.2 cells were mixed with 2×10^5 freshly isolated B6.CD45.1 bone marrow cells and injected via tail vein into lethally irradiated (two doses of 478 cGy over 3 h using a Rad Source RS-2000 X-ray irradiator (Brentwood, TN)) B6.CD45.1$^+$CD45.2$^+$ F1 hybrid recipients. After 8 to 15 weeks, peripheral blood (PB) and bone marrow were analysed.

Lentivirus production, transduction and integration verification. Lentiviral particles were produced by seeding 293 cells at 7×10^5 per cm^2, or PlatE cells (Cell Biolabs, San Diego, CA), in Ultra Culture serum-free media (Lonza, Basel, Switzerland) overnight followed by transfection of each packaging and expression construct (1:1:1) using Trans-It 293 (Mirus, Madison, WI) for 2 h. Media were pooled after 36–48 h, clarified and concentrated by ultracentrifugation (100,000*g*), resuspended in StemPro-34 media and stored at −80 °C. Virus titre was calculated from transduction of NIH-3T3 fibroblasts serial dilutions of the viral preparation. Sorted LT-HSCs were transduced with ≥150 MOI lentivirus particles in the presence of 6 μg ml^{-1} polybrene (Sigma) and spun at 900*g* for 20 min at 20 °C. Supernatant was aspirated and replaced with complete media and cultured overnight. Transduction efficiency of cells was confirmed after 24 h. To assess proviral copy number 15 weeks post-transplantation *in vivo*, splenocytes were harvested and sorted into donor (CD45.2) or competitor (CD45.1) populations and gDNA was isolated as previously described[38]. Amplification of the proviral WPRE region was achieved using SYBR Green qPCR assay using the primer pair WPREFor: 5′-CCGTTGTCAGGCAACGTG-3′ and WPRERev: 5′-AGCTGACAGGTGGTGGCAAT-3′. Quantification of proviral copies was derived from the linear regression of serial dilutions of viral vector and normalized to input cell number.

Quantitative RT–PCR. Sorted or cultured cell populations ($2–5 \times 10^3$ cells) were lysed in TRIzol LS reagent (Invitrogen, Carlsbad, CA) and RNA was isolated according to manufacturer's instructions. cDNA was synthesized using Superscript III Reverse Transcriptase (Invitrogen) and target CT values were determined using inventoried TaqMan probes (Applied Biosystems, Carlsbad, CA, see Supplementary Table 2) spanning exon/exon boundaries and detected using a Viia7 Real Time PCR System (Applied Biosystems). Relative quantification was calculated using the $\Delta\Delta C_T$ method. To estimate relative copy number of *Mfn1* and *Mfn2* transcripts (Fig. 4a), copy numbers were derived from the linear regression of serial dilutions of respective cDNA plasmids and normalized to *GAPDH-VIC* values. To estimate relative copy number of *flPrdm16* transcripts (Fig. 4d), a probe was designed to span the SET methyltransferase domain of *Prdm16* (exon2/3 junction) and copy number was derived from the linear regression of serial dilutions of respective cDNA plasmids. Another probe (exon 14/15 junction) was used to quantify total *Prdm16* copy numbers derived from the linear regression of serial dilutions of respective cDNA plasmids. The values derived from total *Prdm16* probe was subtracted from *flPrdm16*-specific probe to determine *sPrdm16* transcript quantity. All values were normalized to relative multiplexed *GAPDH-VIC* values.

LT-HSC culture. Culture of sorted LT-HSCs was carried out using StemPro34 media (Invitrogen) supplemented with 10 mM HEPES and 50 ng ml^{-1} of recombinant murine SCF, TPO, IL-6 (Peptrotech, Rocky Hill, NJ) and cultured in 5% O_2 at 37 °C. In some experiments, LT-HSCs were cultured in the presence of 500 ng ml^{-1} VIVIT (Millipore, Billerica, MA) or 30 μM mDivi1 (MolPort, Riga, Latvia).

Mitochondrial PEG-1500 fusion assay. To demonstrate a mitochondrial fusion activity, cell fusion experiments were performed using MEFs as previously described[37]. Briefly, BacMam baculovirus constructs (Invitrogen) expressing the signalling peptide from cytochrome *c* fused to either GFP or RFP were transduced separately into MEF cells. Sorted GFP$^+$ and RFP$^+$ MEFs were co-cultured for 24 h

and plasma membranes were fused using PEG-1500 (Roche, Basel, Switzerland. Fused cells were cultured in DMEM containing cyclohexamide (Sigma, St. Louis, MO) for 4 h and analysed for colocalization of mitochondrial labels.

Chromatin immunoprecipitation (ChIP). Early passage *Prdm16*$^{-/-}$ MEFs were transduced with 10 MOI retrovirus for 72 h and fixed with 4% paraformaldehyde for 10 min. Protein lysates were isolated and chromatin immunoprecipitation was carried out using the ChIP-IT Express Enzyme kit (Active Motif, Carlsbad, CA). Antibodies used for ChIP include anti-Flag and anti-TF2D. Primer probes were designed to span regions of the Mfn2 promoter previously shown to regulate *Mfn2* transcriptional activity (see Supplementary Table 3)[39]. Quantification of precipitated Mfn2 promoter regions were derived from the linear regression of serial dilutions of bone marrow genomic DNA, normalized to input DNA concentration and quantifiable IgG detection was subtracted from sample values.

Indo-1-AM calcium flux. Bone marrow was freshly isolated and lineage depleted with the MACS Lineage Depletion Kit (Miltenyi Biotech, San Diego, CA). Cells were cultured for 30 min in complete medium supplemented with 1 μM Indo-1 prepared as stock supplemented with Pluronic-F127 and incubated at 37 °C for 30 min. Cells were washed and stained for surface markers for 15 min, washed and allowed to rest in for 15 min PBS in PBS with Ca^{2+}. FACS tubes were run at 37 °C in the sample port of the LSRII flow cytometer equipped with a 355 nm excitation laser. Events were collected for 40 s before incubation with 25 μM ATP or 1 μM SDF1 to induce calcium transients. The average ratio, *R*, of bound/free Indo-1 (405 nm/485 nm emission) before simulation was used to determine baseline values. Identical samples were equilibrated in 10 mM EGTA PBS without Ca^{2+} to determine R_{min} or stimulated with 1 μM ionomycin to determine R_{max}. The Indo-1 dissociation constant (K_d) was assumed to be 237 nM at 37 °C based on previous studies[40]. The following equation was then used to relate Indo-1 intensity ratios to $[Ca^{2+}]_i$ levels;

$$[Ca^{2+}] = K_d \cdot \frac{(R - R_{min})}{(R_{max} - R)}$$

Immunofluorescence. Sorted or cultured haematopoietic populations ($2–5 \times 10^3$ cells) were collected in complete media and plated on onto MicroWell 96-well glass-bottom plates (Thermo, Waltham, MA) coated with 1ug ml^{-1} poly-D-lysine. Cells were allowed to adhere for 10 min and fixed with 4% PFA for 15 min. Cells were then permeabilized with 0.1% TritonX-100/PBS for 5 min and blocked with 2% BSA/PBS for 1 h at 4 °C. Cells were incubated with anti-Nfat1 (1:100), anti-Mfn2 (1:200), anti-tubulin (1:200), anti CD150-APC (1:100) or anti-Flag (1:250) (see Supplementary Table 1) overnight, washed and incubated with AlexaFluor secondary antibodies (Invitrogen) for 1 h. Cell nuclei were counterstained with DAPI and mounted with fluorescent mounting media (Vector Labs, Burlingame, CA). Confocal images were acquired with a Zeiss LSM 700 confocal microscope or a Leica DMI 6000B and images were deconvoluted and processed with Leica AF6000 software package.

Gene reporter assays. NIH-3T3, WT or *Mfn2*$^{-/-}$ MEF cells were plated at 2×10^4 cells per cm^2 in triplicate overnight and transfected with 500 ng of pGF-Nfat, pGF-CMV or −950/+22 Mfn2-pGL4 reporter construct, 500 ng of cDNA plasmids as indicated and 500 ng of either pSV-βGal or pLVX-IRES-mCherry plasmids with Lipofectamine 3000 according to manufacturer's instructions for 24 or 48 h. Cells were lysed in reporter lysis buffer (Promega, Madison, WI) and analysed for luciferase activity using BrightGlo luciferase (Promega) and detected on a Synergy H2 plate reader (BioTek, Winooski, VT). To visualize βGal activity, cell lysate was incubated in Buffer Z (1mg ml^{-1} ONPG, 0.1 M phosphate, pH 7.5, 10 mM KCl, 1 mM βME, 1 mM $MgSO_4$) at 37 °C for 1 h. Absorbance values were measured at 405 nm and used to normalize for transfection efficiency. In WT and *Prdm16*$^{-/-}$ MEFs, gene reporter luciferase values were normalized to mCherry excitation values.

Western blot. For total cell lysate experiments, MEF cultures were lysed in RIPA buffer, 50 mM Tris pH 7.5, 137 mM NaCl, 0.1% SDS, 0.5% deoxycholate and protease inhibitors (Roche). For subcellular fractionation studies, cells were scraped, washed in PBS. Cell pellets were lysed in 5× packed cell volume (pcv) Buffer A for 10 min on ice and vortexed for 15 s in the presence of 1/10 volume 3% NP-40. Plasma membrane lysis was verified by trypan blue staining. Lysate was spun at 15,000*g* for 10 min at 4 °C and the cytoplasmic fraction was saved. The remaining nuclear pellet was resuspended in 2.5× pc Buffer C and incubated at 4 °C for 1 h with rotation and spun at 15,000*g* for 10 min. The nuclear fraction was diluted with 2.5× volume of Nuclear Diluent Buffer and stored at −80 °C. To achieve even fractionation loading, equivalent percentages of nuclear and cytoplasmic fractions were loaded on each gel. All protein samples were denatured in 4× sample buffer at 95 °C and loaded onto 4–12% Bis-Tris SDS–PAGE gradient gels (Invitrogen). Gels were transferred onto 0.22 μm nitrocellulose membrane and stained with Ruby Red (Molecular Probes, Carlsbad, CA) to confirm transfer. Membranes were blocked with 3% non-fat milk or BSA in 0.1%Tween-20/TBS and incubated with anti-Mfn2 (1:200), anti-βGal (1:1,000), anti-Nfat1 (1:250), anti-tubulin (1:1,000), anti-lamin A/C (1:500) and anti-β-actin (1:5,000) overnight (see Supplementary Table 1). Membranes were washed, incubated with HRPO-conjugated secondary antibodies and exposed to X-ray film (Denville) after incubation with Super Signal West Fempto ECL reagent (Pierce).

Image quantification. For mitochondrial length measurements, confocal or deconvoluted *z*-stacks were collected and projected as a *z*-project in ImageJ (NIH, Bethesda, MD). Individual mitochondria were manually traced, binned into length categories and expressed as percent of cellular mitochondria. The mean ± s.e.m. number of mitochondria falling into each length category collected from ≥ 15 fields (30–50 cells) are expressed. For Nfat nuclear localization quantification, confocal or deconvoluted *z*-stacks were collected and a 1-μm section in the centre of the cell was projected as a *z*-project in ImageJ. Nuclear boundaries were constructed using DAPI staining. The ratio of staining within the nuclear boundary to total staining was expressed as percent of Nfat signal. The mean ± s.e.m. for ≥ 10 fields (20–40 cells) are expressed. For immunofluorescence intensity measurements, confocal or deconvoluted *z*-stacks were collected and projected as a *z*-project in ImageJ. Thresholds were set based on IgG-stained negative control cells and the integrated density value of each signal per cell was recorded. The mean ± s.e.m. for ≥ 15 fields (30–50 cells) are expressed.

Statistics. For statistical analysis between two groups, the unpaired Student's *t*-test was used. When more than two groups were compared, one-way ANOVA was used. Results are expressed as mean ± s.e.m. The Bonferroni and Dunnett multiple comparison tests were used for post-hoc analysis to determine statistical significance between multiple groups. All statistics were calculated using Prism5 (GraphPad, La Jolla, CA) software. Differences among group means were considered significant when the probability value, *P*, was less than 0.05. Sample size ('*n*') always represents biological replicates. Cochran test was used for exclusion of outliers.

No statistical methods were used to predetermine sample size. The experiments were not randomized, and the investigators were not blinded to allocation during experiments and outcome assessment.

31. Zambrowicz, B. P. *et al.* Wnk1 kinase deficiency lowers blood pressure in mice: a gene-trap screen to identify potential targets for therapeutic intervention. *Proc. Natl Acad. Sci. USA* **100,** 14109–14114 (2003).
32. Pham, A. H., McCaffery, J. M. & Chan, D. C. Mouse lines with photo-activatable mitochondria to study mitochondrial dynamics. *Genesis* **50,** 833–843 (2012).
33. Lakso, M. *et al.* Efficient in vivo manipulation of mouse genomic sequences at the zygote stage. *Proc. Natl Acad. Sci. USA* **93,** 5860–5865 (1996).
34. Chen, H., McCaffery, J. M. & Chan, D. C. Mitochondrial fusion protects against neurodegeneration in the cerebellum. *Cell* **130,** 548–562 (2007).
35. Shimshek, D. R. *et al.* Codon-improved Cre recombinase (iCre) expression in the mouse. *Genesis* **32,** 19–26 (2002).
36. Ausubel, F. M. *Current Protocols in Molecular Biology* (Wiley, 1987).
37. Benz, C. *et al.* Hematopoietic stem cell subtypes expand differentially during development and display distinct lymphopoietic programs. *Cell Stem Cell* **10,** 273–283 (2012).
38. Chen, H. *et al.* Mitofusins Mfn1 and Mfn2 coordinately regulate mitochondrial fusion and are essential for embryonic development. *J. Cell Biol.* **160,** 189–200 (2003).
39. Sorianello, E. *et al.* The promoter activity of human Mfn2 depends on Sp1 in vascular smooth muscle cells. *Cardiovasc. Res.* **94,** 38–47 (2012).
40. Grynkiewicz, G., Poenie, M. & Tsien, R. Y. A new generation of Ca^{2+} indicators with greatly improved fluorescence properties. *J. Biol. Chem.* **260,** 3440–3450 (1985).

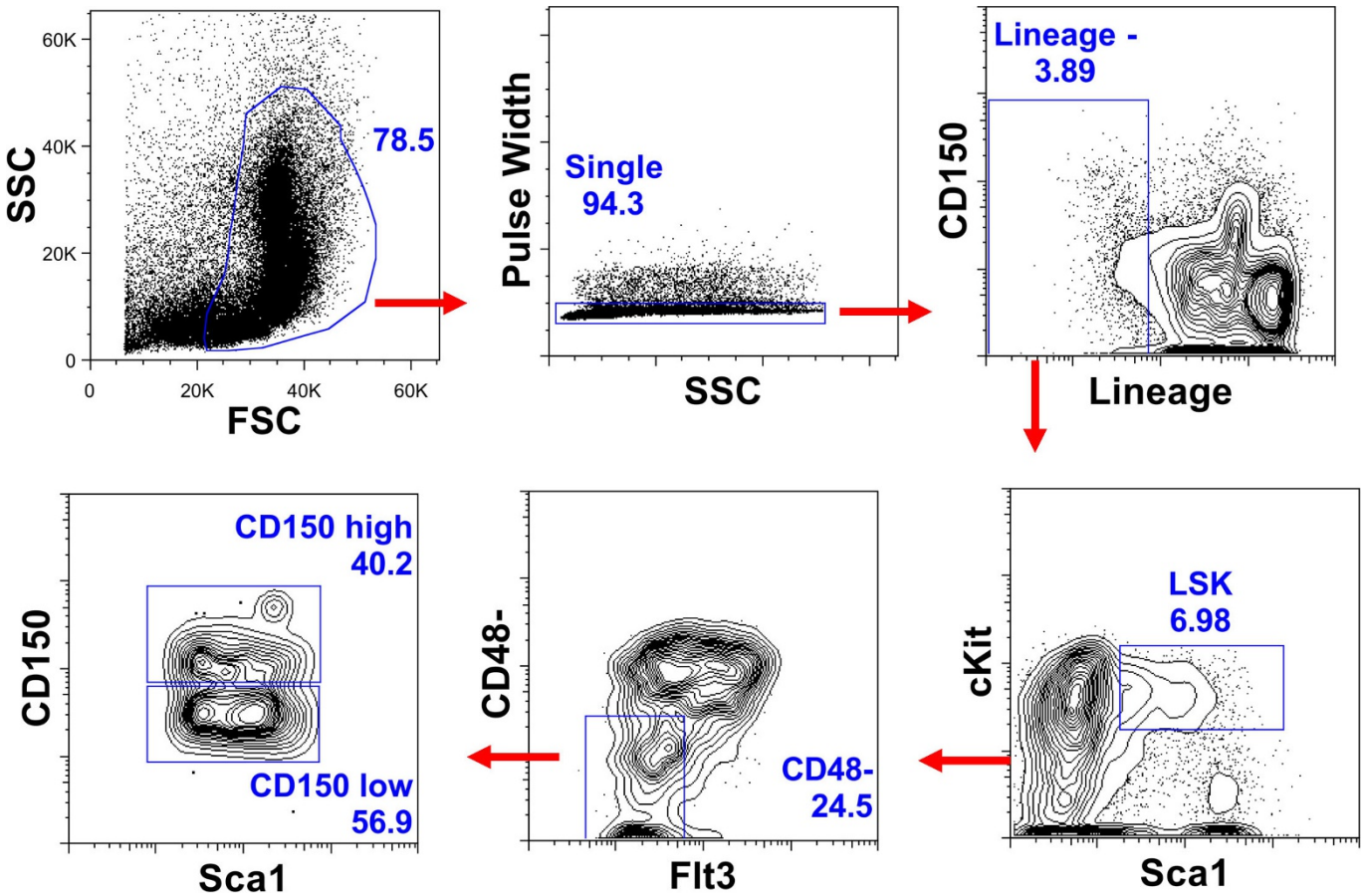

Extended Data Figure 1 | Representative sort gates for isolation of HSCs. Flow cytometric plots showing the gates used to isolate HSCs ($Lin^{-}Sca1^{+}kit^{+}Flt3^{-}CD48^{-}$) and $CD150^{hi}$ and $CD150^{lo}$ HSCs.

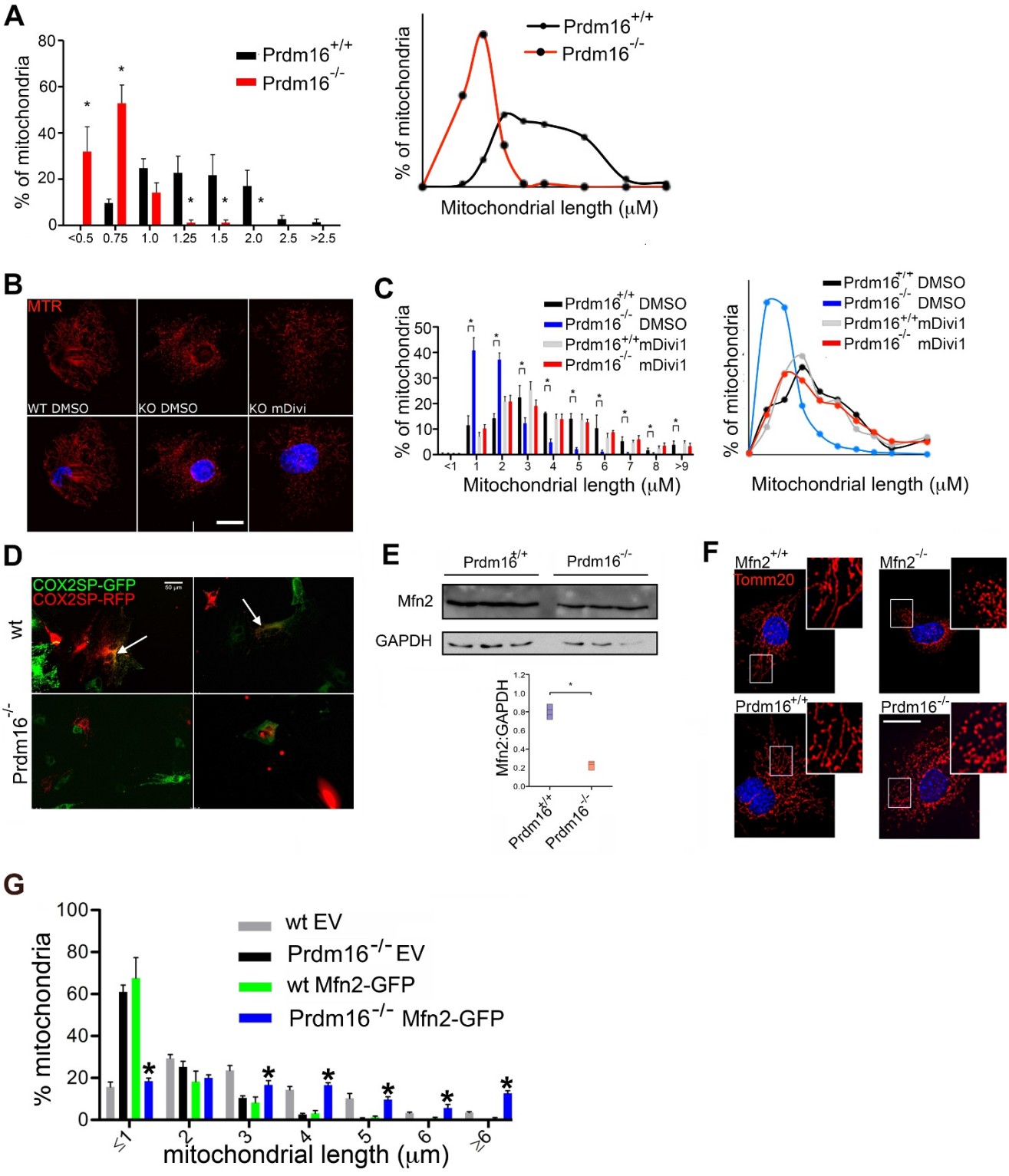

Extended Data Figure 2 | Mitochondrial dynamics in *Prdm16*$^{-/-}$ MEFs. a, Frequency distribution (left) and frequency distribution profile (right) of mitochondrial length in WT or *Prdm16*$^{-/-}$ fetal HSCs. Bars, mean ± s.e.m.; $n \geq 20$ fields of cells from three biological replicates; *$P < 0.05$ within length bins; two-tailed Student's *t*-test within length bins. **b**, Mitochondrial morphology in *Prdm16*$^{-/-}$ MEFs treated for 24 h with the Drp1 inhibitor, mDivi (30 μM), or vehicle is shown for comparison, Mitotracker Red staining, scale bar 20 μm). **c**, Frequency distribution (left) and frequency distribution profile (right) of mitochondrial length in WT and *Prdm16*$^{-/-}$ MEFs treated for 24 h with the Drp1 inhibitor, mDivi (30 μM), or vehicle. Bars, mean ± s.e.m.; $n \geq 16$ fields from three biological replicates; *$P < 0.05$ within length bins; one-way ANOVA with Bonferroni's post-hoc test within length bins. **d**, Fluorescence micrographs showing fusion hybrids of WT or *Prdm16*$^{-/-}$ MEFs transduced with baculovirus expressing mitochondria-tagged GFP and RFP before PEG-mediated fusion (scale bar 50 μm). Fused mitochondria are yellow (arrows), and were only observed in fusions of WT cells. **e**, western blot (upper, Supplementary Fig. 1 for full scans) and quantification of western blots for Mfn2 of WT and *Prdm16*$^{-/-}$ MEFs. Bars, mean ± s.e.m.; $n = 3$ fields biological replicates; *$P < 0.05$; two-tailed Student's *t*-test. **f**, Mitochondrial morphology in WT, *Prdm16*$^{-/-}$ and *Mfn2*$^{-/-}$ MEFs visualized by Tomm20 staining (red) (scale bar 20 μm). **(G)** Mitochondrial length in WT and *Prdm16*$^{-/-}$ MEFs transduced with EV or Mfn2-IRES-GFP (Mfn2–GFP). Bars, mean ± s.e.m.; $n \geq 24$ fields from three biological replicates; *$P < 0.05$ compared to *Prdm16*$^{-/-}$ EV in each length bin; one-way ANOVA with Bonferroni's post-hoc test within length bins.

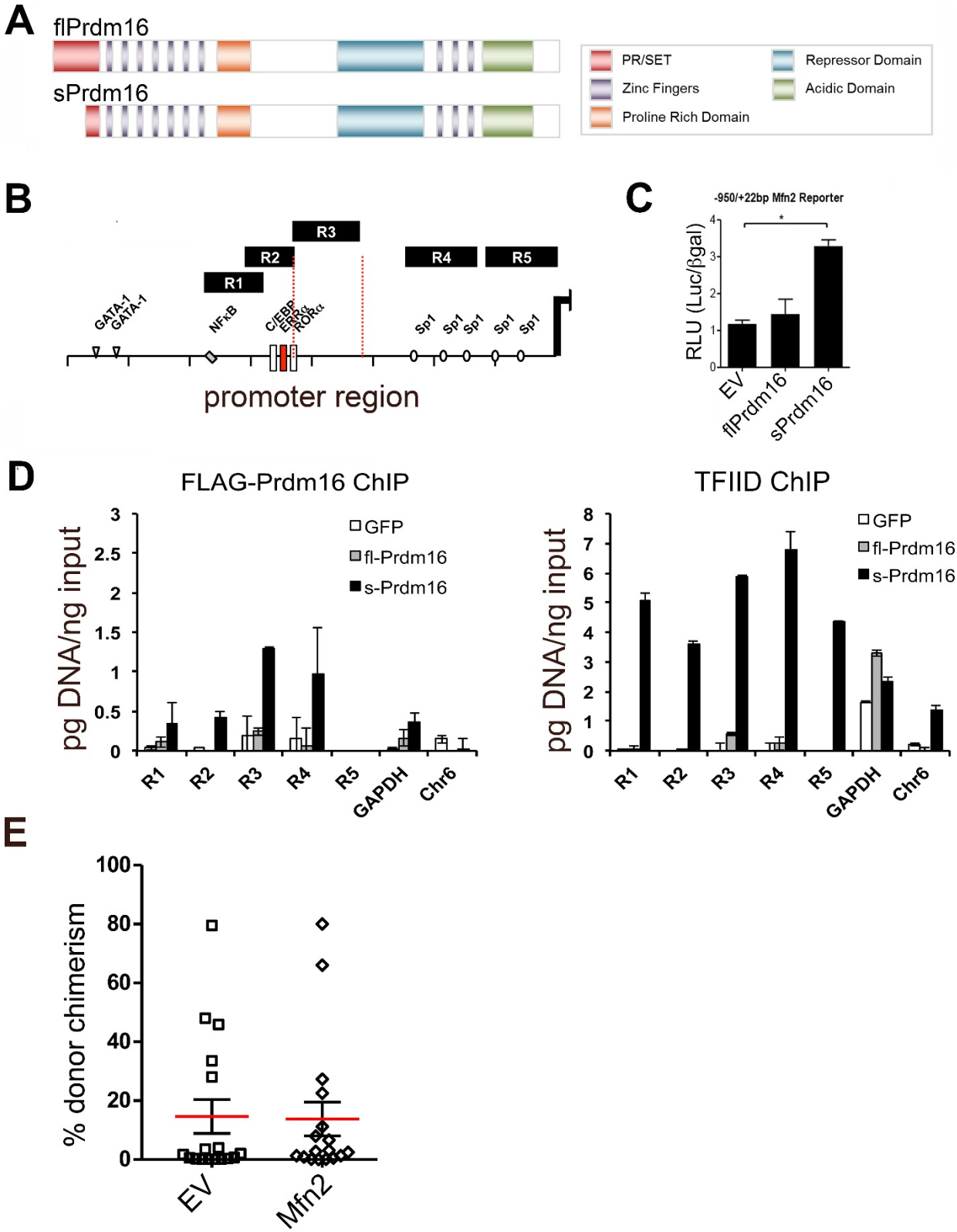

Extended Data Figure 3 | sPrdm16 interacts with the Mfn2 promoter. **a**, Schematic representation of Prdm16 protein domain structure. **b**, qPCR probe amplification scheme covering the Mfn2 promoter used in chromatin immunoprecipitation assays. **c**, Proximal Mfn2 promoter luciferase gene reporter assay in WT MEFs transfected 24 h previously with flPrdm16, sPrdm16 or control vectors. Bars, mean ± s.e.m.; $n = 3$ biological replicates; $^*P < 0.05$; one-way ANOVA with Dunnett's post-hoc test. **d**, ChIP quantification in *Prdm16*$^{-/-}$ MEFs transduced with retroviral Flag–Prdm16 constructs immunoprecipitated using Flag and TF2D antibodies. TFIID positive (GAPDH) and negative (intergenic Chr 6) control probes are also shown. Quantification was performed after establishment of qPCR standard curves for all probes (see Methods). Bars, mean ± s.e.m.; $n = 3$ technical replicates representative tow biological replicates; $^*P < 0.05$; one-way ANOVA with Dunnett's post-hoc test. **e**, Percentage CD45.2 (donor) contribution in PB WBC in CD45.1$^+$CD45.2$^+$ mice reconstituted with 200 transduced (IRES–GFP or Mfn2-IRES–GFP) *Prdm16*$^{+/-}$ CD45.2$^+$ HSCs and 2×10^5 CD45.1$^+$ competitor bone marrow cells. Plots, mean ± s.e.m.; $n = 17$ recipients pooled from four independent transplants; $^*P < 0.05$; two-tailed Student's *t*-test.

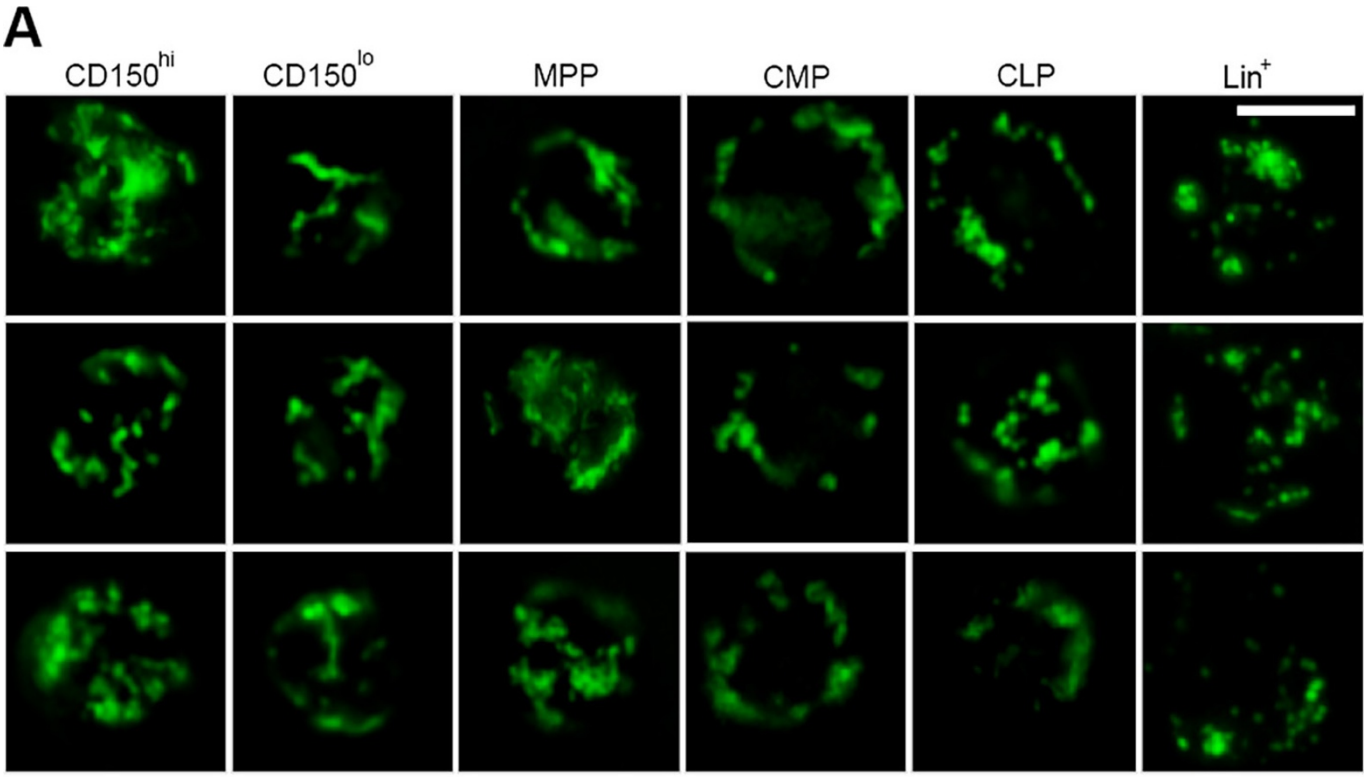

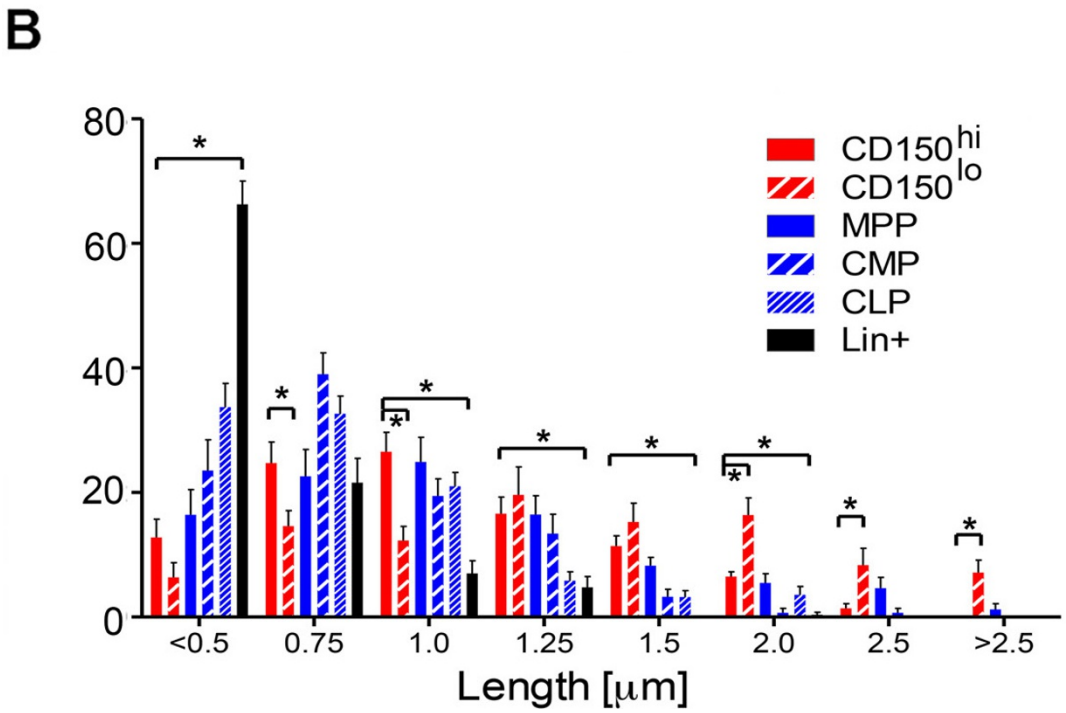

Extended Data Figure 4 | Mitochondrial morphology of bone marrow populations. a, Representative images of mitochondrial morphology in Pham-reporter^{+} CD150^{hi} and CD150^{lo} HSCs (lin^{-}Sca1^{+}kit^{+}Flt3^{-}CD48^{-}), MPPs (lin^{-}Sca1^{+}kit^{+}CD48^{+}), CMPs (lin^{-}Sca1^{-}kit^{+}), CLPs (lin^{-}Sca1^{lo}kit^{lo}IL7Ra^{+}Flt3^{+}) and lineage^{+} cells (scale bar, 5 μm). **b**, Mitochondrial length frequency distribution in Pham-reporter^{+} HSCs, progenitors and Lin^{+} cells. Bars, mean ± s.e.m.; $n \geq 14$ fields from three biological replicates; *$P < 0.05$ within length bins; one-way ANOVA with Bonferroni's post-hoc test within length bins.

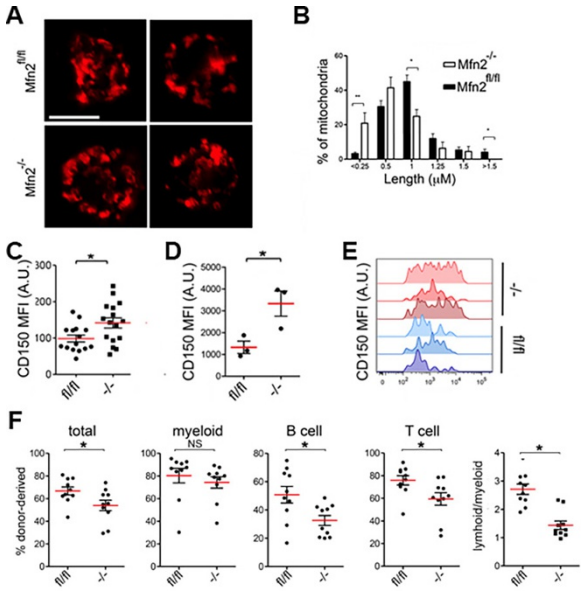

Extended Data Figure 5 | Phenotype and function of *Mfn2*$^{-/-}$ HSCs. **a**, Mitochondrial morphology HSCs from *Mfn2*$^{fl/fl}$ or *Mfn2*$^{fl/fl}$-*Vav-Cre* (*Mfn2*$^{-/-}$) mice visualized with immunostaining for Tomm20. **b**, Frequency distribution of mitochondrial lengths (right panel, compared to WT in each length bin). Bars, mean ± s.e.m.; $n \geq 7$ fields from two biological replicates; $^{*}P < 0.05$ within length bins; two-tailed Student's *t*-test within length bins. **c**, CD150 surface staining mean fluorescence intensity (MFI) of HSCs (Lin^{-}Sca1^{+}kit^{+}CD48^{-}) in 8–12 week old *Mfn2*$^{fl/fl}$ or *Mfn2*$^{fl/fl}$.*Vav-Cre* (*Mfn2*$^{-/-}$) mice. $n = 25$ biological replicates, $^{*}P < 0.05$, two-tailed Student's *t*-test. **d**, **e**, CD150 MFI of *Mfn2*$^{fl/fl}$ or *Mfn2*$^{fl/fl}$. *Vav-Cre* (*Mfn2*$^{-/-}$) donor HSCs 15 weeks after competitive transplantation. Plots in **d**, mean ± s.e.m.; $n \geq 15$ mice from three biological replicates. **f**, $^{*}P < 0.05$; two-tailed Student's *t*-test. **f**, Donor (CD45.2) chimaerism 15 weeks after competitive transplantation of 2×10^5 *Mfn2*$^{fl/fl}$ or *Mfn2*$^{fl/fl}$.*Vav-Cre* (*Mfn2*$^{-/-}$) fetal liver cells together with 2×10^5 CD45.1^{+} competitor bone marrow cells into CD45.1^{+}CD45.2^{+} recipients Plots, mean ± s.e.m.; $n = 10$ mice pooled from two independent transplants; $^{*}P < 0.05$; two-tailed Student's *t*-test.

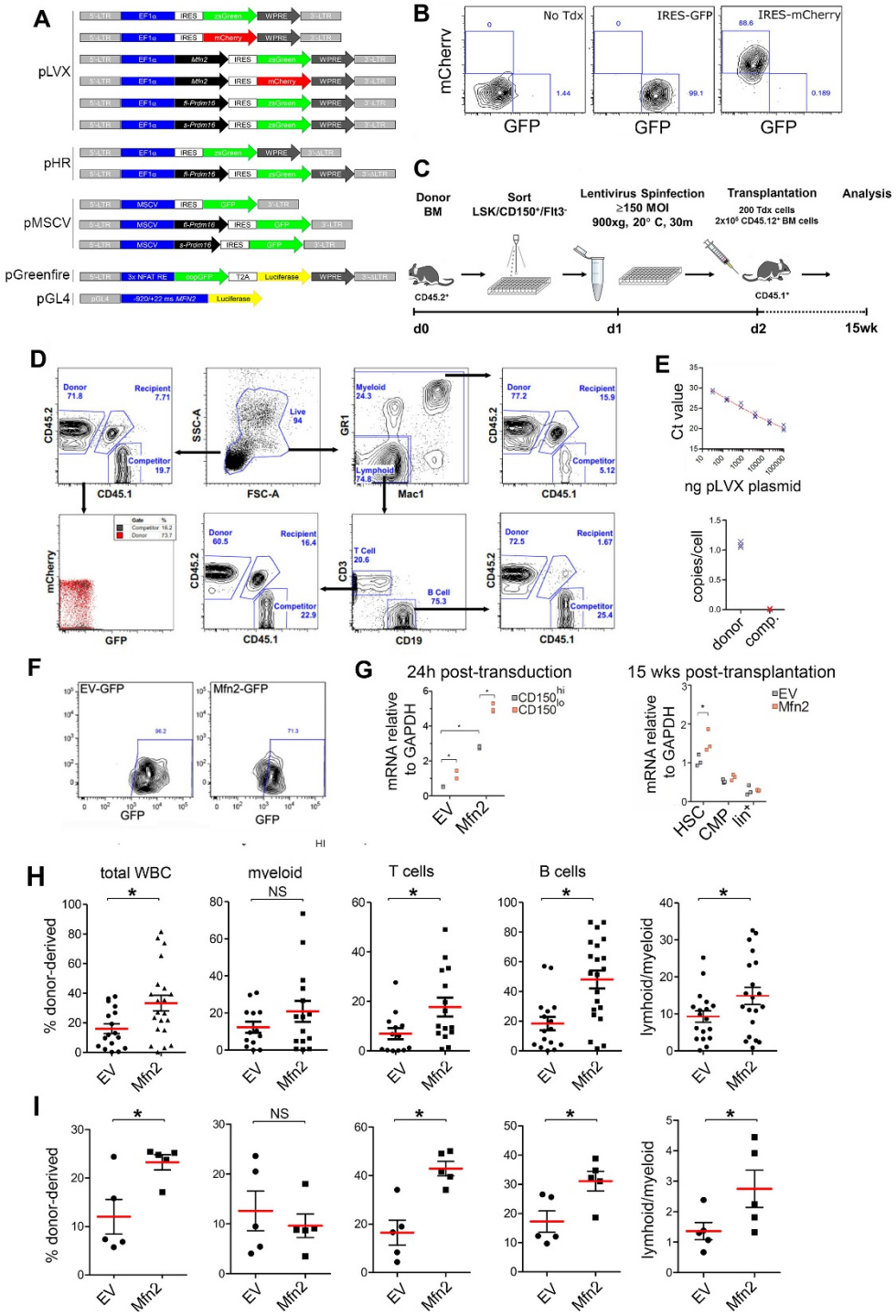

Extended Data Figure 6 | Analysis of competitive repopulation experiments and lentiviral vector transduction. a, Schematic representation of lentiviral constructs used. **b**, Representative example of transduction efficiency of purified HSCs with IRES–GFP and IRES–mCherry vectors 24–48 h post-transduction. **c**, Schematic representation of transduction and subsequent competitive repopulation experiments. **d**, Representative flow cytometric plots of the gates used to analyse recipients of competitive repopulation experiments. The CD45.1/CD45.2 gates were also applied to the myeloid, B and T cell gates to determine donor contribution to individual lineages. In this example, HSCs had been transduced with an IRES–GFP lentiviral vectors (efficiency 80%, see **b**). Although donor repopulation was high in the periphery (upper left panel, 71.8%) no GFP was detected (lower left panel), suggesting silencing of the vectors. **e**, Quantification of proviral copy number in donor-derived ($CD45.2^+$) 15 weeks after transduction and competitive transplantation of HSCs. Despite silencing of the vector (see **d**), approximately 1 proviral copy was present per donor HSC-derived cell. $n = 3$ biological replicates; $^*P < 0.05$; two-tailed Student's *t*-test. **f**, Representative example of transduction efficiency of purified HSCs with IRES–GFP and Mfn2–IRES–GFP lentiviral vectors. **g**, Expression of *Mfn2* mRNA in $CD150^{hi}$ and $CD150^{lo}$ HSCs 24 h post-transduction relative to EV control (left panel) and in donor-derived HSCs, CMPs and $lineage^+$ cells 15 weeks after competitive transplantation of 200 transduced HSCs together with 2×10^5 $CD45.1^+$ competitor cells (right panel). The data indicate partial silencing of the vector in HSCs, and complete silencing in the progenitors and more mature cells. $n = 3$ biological replicates; $^*P < 0.05$; two-way analysis of variance (ANOVA) with Bonferroni's post-hoc test. **h**, Donor ($CD45.2^+$) chimaerism 15 weeks after transplantation of 200 $CD45.2^+$ HSCs transduced for 24 h with SIN LTR constructs pLVX-IRES-GFP or pLVX-Mfn2-IRES-GFP together with 2×10^5 $CD45.1^+$ competitor fetal liver cells into lethally irradiated $CD45.1^+CD45.2^+$ recipients mice. Plots, mean ± s.e.m.; $n \geq 19$ recipients from four transplantation experiments; $^*P < 0.05$; two-tailed Student's *t*-test. **i**, Same experiments as in **h**, but using the non-SIN LTR vector, pHR. Plots, mean ± s.e.m.; $n = 5$ recipients; $^*P < 0.05$; two-tailed Student's *t*-test.

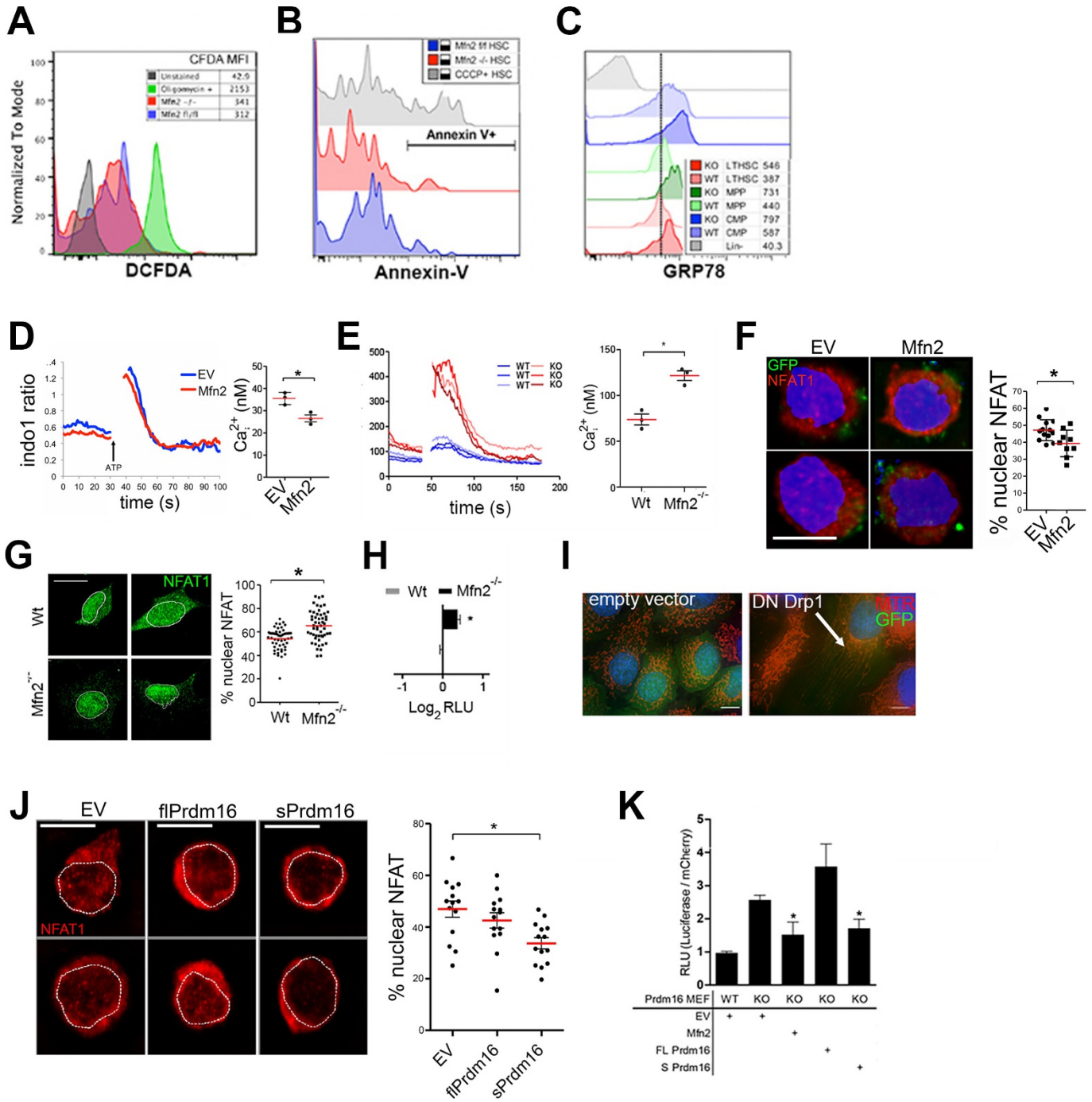

Extended Data Figure 7 | Nfat activity in *Mfn2*$^{-/-}$ and *Prdm16*$^{-/-}$ MEFs. a, *Mfn2*$^{fl/fl}$ (blue) or *Mfn2*$^{fl/fl}$-*Vav-Cre* (*Mfn2*$^{-/-}$) (red) HSCs were stained with DCFDA to visualize intracellular reactive oxygen species levels. Cells were treated with oligomycin for 15 min as a positive control. **b**, HSC apoptosis levels were analysed by surface staining of Annexin V. **c**, Intracellular staining for the endoplasmic reticulum stress response chaperone GRP78 in *Mfn2*$^{fl/fl}$ or *Mfn2*$^{fl/fl}$-*Vav-Cre* (*Mfn2*$^{-/-}$) HSCs (red colours) MPPs (green colours) and CMPs (blue colours). Histograms; representative of three biological replicates. **d**, Calcium flux trace (left) and baseline intracellular Ca^{2+} (right) in WT LSK cells transduced with IRES–GFP or Mfn2–IRES–GFP lentiviral vectors (**e**) and with WT or *Mfn2*$^{-/-}$ MEFs stained with Indo1. Bars, mean ± s.e.m.; $n = 3$ biological replicates; $^*P < 0.05$; two-tailed Student's *t*-test. **f**, Nfat1 staining (left, scale bars, 5 μm) and fraction of nuclear Nfat1 (right, $^*P < 0.05$) in HSCs transduced with IRES–GFP or Mfn2–IRES–GFP lentiviral vector. Bars, mean ± s.e.m.; $n \geq 10$ from two biological replicates; $^*P < 0.05$; two-tailed Student's *t*-test. **g**, Nfat1 staining (left; scale bars, 20 μm) and fraction of nuclear Nfat1 (right; $^*P < 0.05$) in WT or *Mfn2*$^{-/-}$ MEFs. Bars, mean ± s.d.; $n \geq 20$ fields from three independent experiments; $^*P < 0.05$; two-tailed Student's *t*-test. **h**, Nfat luciferase gene reporter activity in WT or *Mfn2*$^{-/-}$ MEFs. Bars, mean ± s.d.; $n = 3$ experiments; $^*P < 0.05$; two-tailed Student's *t*-test. **i**, Mitochondrial morphology after transfection of dominant negative Drp1 into HeLa cells (scale bars, 5 μm). Note extreme elongation of mitochondria (arrow), confirming that this vector is functional. **j**, Nfat1 staining (left, scale bars, 5 μm) and fraction of nuclear Nfat1 (right) in HSCs lentivirally transduced with sPRrdm16 and flPRdm16. Plots, mean ± s.e.m.; $n \geq 14$ fields of cells pooled from two biological replicates; $^*P < 0.05$; one-way ANOVA with Dunnett's post-hoc test. **k**, Nfat luciferase gene reporter activity in WT and in *Prdm16*$^{-/-}$ MEFs transfected with Mfn2, flPrdm16 or sPrdm16 constructs. Bars, mean ± s.d.; $n = 3$ experiments; $^*P < 0.05$; one-way ANOVA with Dunnett's post-hoc test.

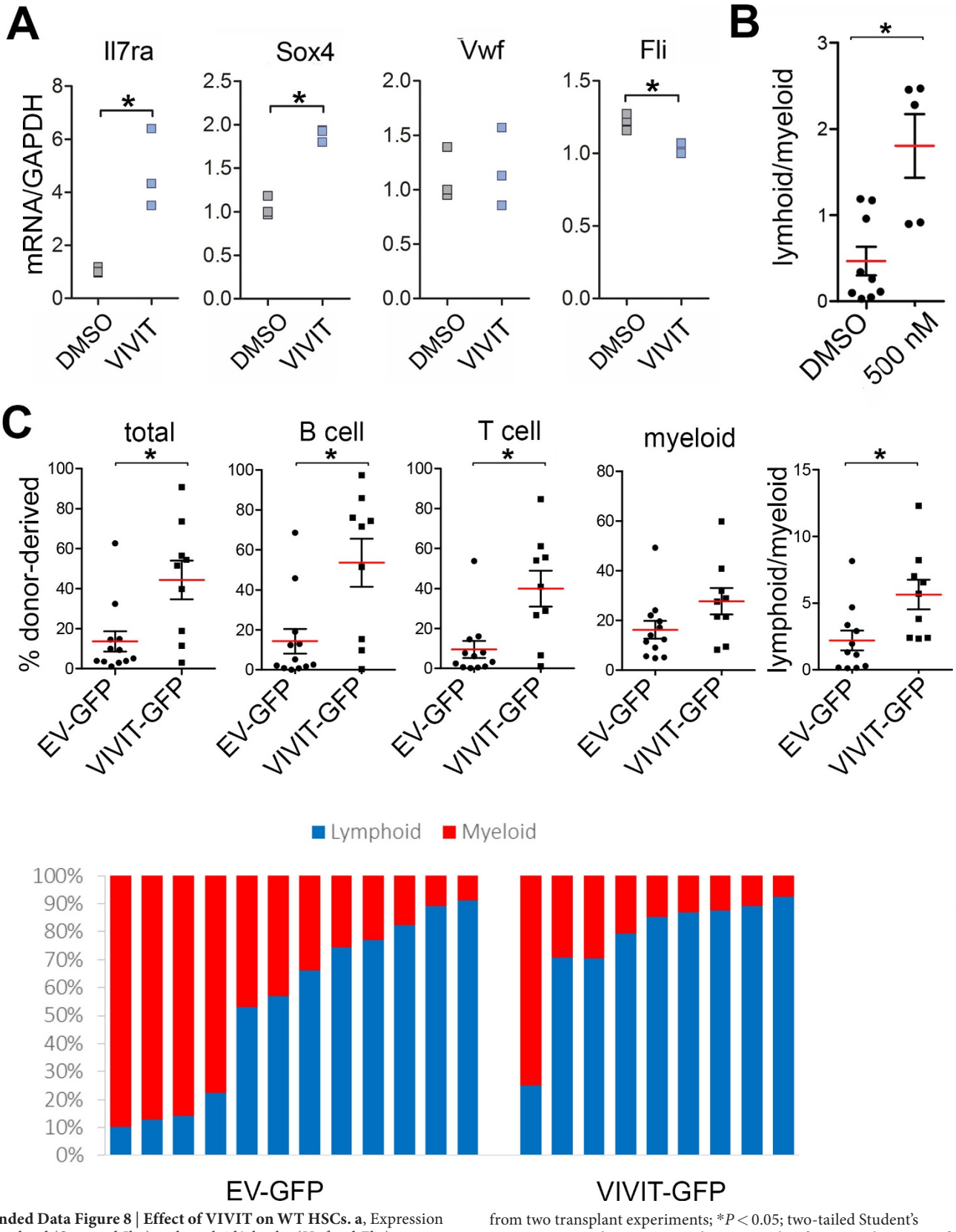

Extended Data Figure 8 | Effect of VIVIT on WT HSCs. a, Expression of lymphoid (*Sox4* and *Il7r*) and myeloid/platelet (*Vwf* and *Fli1*) genes in HSCs treated with VIVIT or DMSO for 24 h. $n = 3$ biological replicates; $^*P < 0.05$; Student's *t*-test. **b**, Lymphoid/myeloid ratio of CD45.2$^+$ HSCs cultured for 4 days in DMSO and 500 nM VIVIT, transplanted with 2×10^5 CD45.1$^+$CD4^5.2$^+$ competitor bone marrow cells into CD45.1$^+$ recipients and analysed 15 weeks post-transplant for lymphoid/myeloid ratio of donor compartment. Plots, mean ± s.e.m.; $n = 5$–9 recipients from two transplant experiments; $^*P < 0.05$; two-tailed Student's *t*-test. **c**, Donor chimaerism analysis 15 weeks after transplantation of CD45.2$^+$ HSCs transduced with IRES–GFP or VIVIT–GFP with 2×10^5 CD45.1$^+$CD45.2$^+$ competitor bone marrow cells into CD45.1$^+$ recipients Plots, mean ± s.e.m.; $n = 9$–12 recipients from two independent transplant experiments; $^*P < 0.05$; two-tailed Student's *t*-test. Bottom panel shows lymphoid and myeloid donor contribution in each individual recipient.

Extended Data Table 1 | Phenotypic analysis of the haematopoietic system in *Mfn2$^{fl/fl}$-Vav-Cre* mice

A

Hematopoietic Stem Cell Compartments		
	LSK	LSK CD48- Flt3- CD150+
Mfn2 f/f		
	0.277%	0.053%
	0.319%	0.082%
	0.346%	0.058%
Mean	*0.314% ± 0.03*	***0.064% ± 0.02****
Mfn2 f/f Vav-Cre		
	0.213%	0.021%
	0.575%	0.047%
	0.220%	0.039%
Mean	*0.336% ± 0.20*	***0.036% ± 0.01****

B

Peripheral blood counts

	WT	*KO*
N=	*8*	*4*
WBC	7.3 ± 2.6	8.7 ± 1.7
Neutrophil %	15.4 ± 9.2	15.4 ± 12.0
Lymphocytes%	73.0 ± 12.8	78.2 ± 12.6
Monocytes %	6.2 ± 2.8	5.9 ± 3.2
Eosinophiles%	0.4 ± 0.3	1.3 ± 1.4
Basophiles %	0.1 ± 0.1	0.4 ± 0.4
NRBC%	±	±
Hematocrit	45.1 ± 4.2	45.3 ± 6.7
RBC	8.7 ± 0.7	8.9 ± 1.2
HB	12.3 ± 1.2	12.8 ± 1.6
MCV	51.5 ± 1.7	50.7 ± 1.8
MCH	14.1 ± 0.5	14.4 ± 0.5
MCHC	27.3 ± 0.8	28.4 ± 0.7
RDW	15.2 ± 1.7	15.5 ± 1.4
RSD	7.9 ± 0.9	7.9 ± 0.9
RETIC#	47.4 ± 29.9	49.1 ± 42.0
RETIC%	0.6 ± 0.4	0.6 ± 0.5
Platelet	642.8 ± 146.4	653.0 ± 66.7

C

Bone Marrow Progenitor Compartments					
	MPP	GMP	CMP	MEP	CLP
Mfn2 f/f					
		0.00272%	0.00184%	0.00281%	0.00049%
		0.00841%	0.00469%	0.00958%	0.00067%
		0.00149%	0.00164%	0.00135%	0.00409%
Mean	*0.314% ± 0.03*	*0.0042% ± 4e-5*	*0.0027% ± 2e-5*	*0.0046% ± 4e-5*	*0.00175% ± 2e-5*
Mfn2 f/f Vav-Cre					
		0.00321%	0.00224%	0.00369%	0.00108%
		0.00844%	0.00550%	0.00589%	0.00041%
		0.00136%	0.00110%	0.00142%	0.00916%
Mean	*0.336% ± 0.20*	*0.0043% ± 4e-5*	*0.0029% ± 2e-5*	*0.0037% ± 2e-5*	*0.00355% ± 5e-5*

D

Splenocyte Lineages			
	Mac1+ or GR1+	CD3+	CD19+
Mfn2 f/f			
	6.840%	17.60000%	59.70000%
	9.910%	27.80000%	63.70000%
	8.375%	22.700%	61.700%
Mean	*8.37% ± 0.02*	*22.70% ± 0.05*	*61.70% ± 0.02*
Mfn2 f/f Vav-Cre			
	11.800%	13.79000%	62.59000%
	9.070%	27.50000%	63.20000%
	10.435%	20.645%	62.895%
Mean	*10.43% ± 0.01*	*20.65% ± 0.07*	*62.90% ± 0.01*

E

Peripheral Blood Lineages			
	Mac1+ or GR1+	CD3+	CD19+
Mfn2 f/f			
	26.300%	9.75280%	54.75000%
	23.100%	26.800%	42.135%
	19.900%	43.84800%	29.51910%
Mean	*23.1% ± 0.03*	*26.8% ± 17*	*42.1% ± 13*
Mfn2 f/f Vav-Cre			
	15.200%	15.63765%	63.22500%
	17.900%	35.944%	41.143%
	20.600%	56.24940%	19.06100%
Mean	*17.9% ± 0.02*	*35.9% ± 20*	*62.9% ± 22*

F

Thymus Lineages								
	CD4	CD8	DP	DN	DN1	DN2	DN3	DN4
Mfn2 f/f								
	10.50%	2.95%	81.60%	2.11%	0.03%	0.10%	0.54%	0.19%
	11.10%	2.10%	81.30%	3.10%	0.04%	0.15%	0.81%	0.17%
	5.95%	3.01%	83.20%	1.48%	0.03%	0.10%	0.41%	0.06%
Mean	*9.2% ± 2.8*	*2.7% ± 0.5*	*82.1% ± 1.0*	*2.2% ± 0.8*	*0.33% ± 0.006*	*0.117% ± 0.03*	*0.587% ± 0.20*	*0.14% ± 0.07*
Mfn2 f/f Vav-Cre								
	9.42%	2.56%	83.00%	1.86%	0.03%	0.13%	0.54%	0.20%
	9.25%	2.55%	84.50%	2.09%	0.06%	0.13%	0.81%	0.20%
	11.30%	3.44%	80%	2.74%	0.03%	0.09%	0.57%	0.21%
Mean	*10.0% ± 1.1*	*2.8% ± 0.5*	*82.5% ± 2.3*	*2.2% ± 0.5*	*0.040% ± 0.02*	*0.117% ± 0.02*	*0.64% ± 0.15*	*0.203% ± 0.01*

a–**f**, Analysis of 8–10 week-old *Mfn2$^{fl/fl}$* or *Mfn2$^{fl/fl}$-Vav-Cre* mice for (**a**) frequency of LSK cells and HSCs, (**b**) peripheral blood counts, (**c**) bone marrow progenitor populations (MPPs (lin$^-$Sca1$^+$kit$^+$CD48$^+$), CMPs (lin$^-$Sca1$^-$kit$^+$), CLPs (lin$^-$Sca1^{lo}kit^{lo}IL7Ra$^+$Flt3$^+$), MEPs (Lin$^-$Kit$^+$Sca1$^-$CD16/32^{low}CD34$^-$)), (**d**) myeloid (Gr1$^+$/Mac1$^+$), T (CD3$^+$) and B (CD19$^+$) cells in the spleen, (**e**) myeloid (Gr1$^+$/Mac1$^+$), T (CD3$^+$) and B (CD19$^+$) cells in peripheral blood mononuclear cells, and (**f**) thymocyte subpopulations (DP: CD4$^+$CD8$^+$, DN: CD4$^-$CD8$^-$, DN1: CD4$^-$CD8$^-$CD44$^+$CD25$^-$, DN2: CD4$^-$CD8$^-$CD44$^+$CD25$^+$, DN3: CD4$^-$CD8$^-$CD44$^-$CD25$^+$, DN4: CD4$^-$CD8$^-$CD44$^-$CD25$^-$). Data are mean ± s.e.m.; $n = 3$ mice; *$P < 0.05$; two-tailed Student's *t*-test.

Extended Data Table 2 | Statistical analysis of limiting dilution experiments shown in Fig. 3c

total reconstitution			
Group	Lower	Estimate	Upper
KO	108.1	55.6	28.72
WT	30.3	17	9.59
Chisq	DF	P.value	
7.64	1	0.00571	

lymphoid reconstitution			
Group	Lower	Estimate	Upper
KO	407.6	153.2	57.8
WT	69.8	38.2	21
Chisq	DF	P.value	
6.71	1	0.00957	

myeloid reconstitution			
Group	Lower	Estimate	Upper
KO	35.8	20.23	11.5
WT	18.5	8.96	4.5
Chisq	DF	P.value	
3.1	1	0.0785	